Quantitative Analysis of Mitochondrial Ca^{2+} Uptake and Release Pathways in Sympathetic Neurons

Reconstruction of the Recovery after Depolarization-evoked $[Ca^{2+}]_i$ Elevations

Stephen L. Colegrove, Meredith A. Albrecht, and David D. Friel

From the Department of Neuroscience, Case Western Reserve University, Cleveland, Ohio

abstract Rate equations for mitochondrial Ca^{2+} uptake and release and plasma membrane Ca^{2+} transport were determined from the measured fluxes in the preceding study and incorporated into a model of Ca^{2+} dynamics. It was asked if the measured fluxes are sufficient to account for the $[Ca^{2+}]_i$ recovery kinetics after depolarization-evoked $[Ca^{2+}]_i$ elevations. Ca^{2+} transport across the plasma membrane was described by a parallel extrusion/leak system, while the rates of mitochondrial Ca^{2+} uptake and release were represented using equations like those describing Ca^{2+} transport by isolated mitochondria. Taken together, these rate descriptions account very well for the time course of recovery after $[Ca^{2+}]_i$ elevations evoked by weak and strong depolarization and their differential sensitivity to FCCP, CGP 37157, and $[Na^+]_i$. The model also leads to three general conclusions about mitochondrial Ca^{2+} transport in intact cells: (1) mitochondria are expected to accumulate Ca^{2+} even in response to stimuli that raise $[Ca^{2+}]_i$ only slightly above resting levels; (2) there are two qualitatively different stimulus regimes that parallel the buffering and non-buffering modes of Ca^{2+} transport by isolated mitochondria that have been described previously; (3) the impact of mitochondrial Ca^{2+} transport on intracellular calcium dynamics is strongly influenced by nonmitochondrial Ca^{2+} transport; in particular, the magnitude of the prolonged $[Ca^{2+}]_i$ elevation that occurs during the plateau phase of recovery is related to the Ca^{2+} set-point described in studies of isolated mitochondria, but is a property of mitochondrial Ca^{2+} transport in a cellular context. Finally, the model resolves the paradoxical finding that stimulus-induced $[Ca^{2+}]_i$ elevations as small as ~300 nM increase intramitochondrial total Ca^{2+} concentration, but the steady $[Ca^{2+}]_i$ elevations evoked by such stimuli are not influenced by FCCP.

key words: mitochondria • calcium • neurons • Ca^{2+} uniporter • mitochondrial Na^+/Ca^{2+} exchanger

INTRODUCTION

Ionized free calcium (Ca^{2+}) is an important signal that links a variety of extracellular stimuli to their intracellular effectors. Since Ca^{2+} accomplishes this function by interacting with Ca^{2+} binding proteins, the cellular effects of Ca^{2+} depend critically on the dynamics of Ca^{2+} concentration ($[Ca^{2+}]$). One of the central goals in the study of calcium signaling is to understand the basis of $[Ca^{2+}]$ dynamics. This is complicated by several factors: (a) Ca^{2+} is present in multiple membrane-delimited intracellular compartments, each of which employs distinctive Ca^{2+} transport systems; (b) Ca^{2+} may be distributed in a spatially nonuniform manner within these compartments; (c) the rate of Ca^{2+} transport between compartments can exhibit a complex nonlinear dependence on free Ca concentration.

We have studied how mitochondrial Ca^{2+} transport contributes to the redistribution of intracellular Ca^{2+} during and after depolarization-evoked Ca^{2+} entry in sympathetic neurons. Here, the rise in cytosolic free Ca^{2+} concentration ($[Ca^{2+}]_i$) is initiated by Ca^{2+} entry but is strongly influenced by Ca^{2+} uptake and release by organelles such as mitochondria and the endoplasmic reticulum (ER).[1] We simplified the analysis of $[Ca^{2+}]$ dynamics by inhibiting SERCA Ca^{2+} pumps to minimize Ca^{2+} accumulation by the ER, and by focusing on the slow recovery that follows repolarization, a period during which the spatial distribution of $[Ca^{2+}]_i$ is approximately uniform. Analysis of this case is relevant to slow changes in $[Ca^{2+}]$ that occur in the aftermath of depolarizing stimuli, and is a logical step in understanding the more complex case where $[Ca^{2+}]$ undergoes rapid, spatially nonuniform changes within multiple intracellular compartments.

In the preceding study, the total Ca^{2+} flux during the recovery after depolarization was dissected into three components, one representing net Ca^{2+} extrusion across the plasma membrane, the others representing mito-

Address correspondence to David Friel, Ph.D., Department of Neuroscience, Case Western Reserve University, 10900 Euclid Ave. Cleveland, OH 44106. Fax: (216) 368-4650; E-mail: ddf2@po.cwru.edu

[1]*Abbreviations used in this paper:* ER, endoplasmic reticulum; Tg, thapsigargin.

J. Gen. Physiol. © The Rockefeller University Press • 0022-1295/2000/03/371/18 $5.00
Volume 115 March 2000 371–388
Released online 28 February 2000
http://www.jgp.org/cgi/content/full/115/3/371

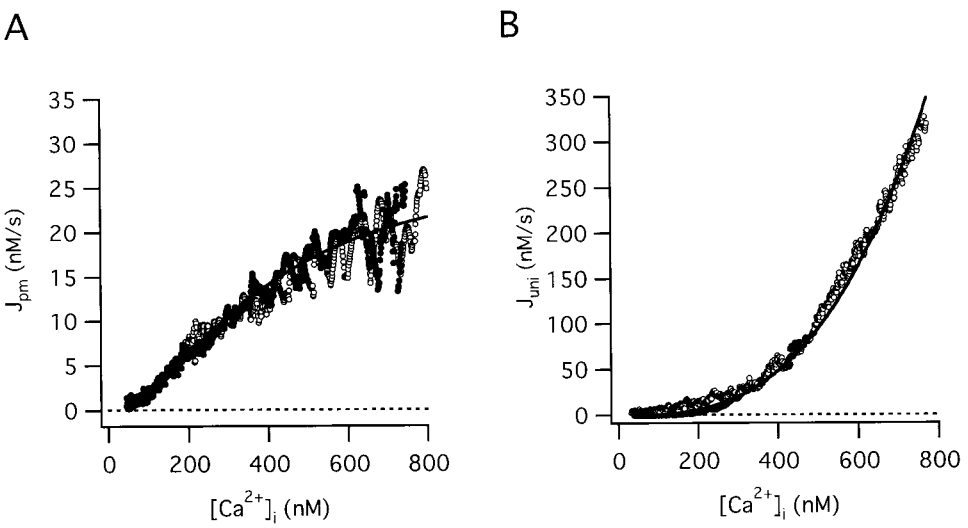

Figure 1. Quantitative description of the $[Ca^{2+}]_i$-dependent transport pathways: J_{pm} and J_{uni}. (A) $[Ca^{2+}]_i$ dependence of J_{pm}. Mean J_{pm} from ten cells plotted against $[Ca^{2+}]_i$ (solid symbols). The total Ca^{2+} flux during the recovery was measured after 50 mM K^+ depolarization in the presence of FCCP (1 μM). J_{pm} can be described by Eq. 1 (smooth curve) with: $k_{leak} = 3.7 \times 10^{-7}$ s^{-1}, $V_{max,extru} = 28.3$ nM/s, $EC_{50,extru} = 378.8$ nM and $n_{extru} = 1.8$. This equation also describes mean J_{pm} from three cells studied under voltage clamp after adjusting for differences in resting $[Ca^{2+}]_i$ by subtracting a small constant leak flux (−5 nM/s, open symbols). (B) $[Ca^{2+}]_i$ dependence of $J_{uni.}$ Mean J_{uni} from three cells studied under voltage clamp plotted against $[Ca^{2+}]_i$ (open symbols). Cells were depolarized from −70 to −10 mV before and after exposure to FCCP (1 μM) and J_{uni} was calculated as the difference between the net Ca^{2+} fluxes at corresponding values of $[Ca^{2+}]_i$ during the recovery. Pipette solutions contained no added Na^+ to inhibit mitochondrial Ca^{2+} release via the Na^+/Ca^{2+} exchanger. Data are described by Eq. 2 (smooth curve) with $k_{max,uni} = 75.9$ s^{-1}, $EC_{50,uni} = 10$ μM and $n_{uni} = 2$, which also provides a good description of J_{uni} after 50 mM K^+ depolarization (filled symbols, mean J_{uni} from ten cells measured for $[Ca^{2+}]_i$ up to ∼500 nM).

chondrial Ca^{2+} uptake and release via the uniporter and Na^+/Ca^{2+} exchanger. In this study, these flux components are described analytically to determine if they are sufficient to account for the time course of the $[Ca^{2+}]_i$ recovery after weak and strong stimuli, and the effects of mitochondrial Ca^{2+} transport inhibitors on these recoveries. It is found that they are. Moreover, the results are in general quantitative agreement with the dynamics of total mitochondrial Ca concentration deduced from x-ray microanalysis under the same conditions of stimulation. The results provide a conceptual framework for describing how mitochondrial Ca transport operates in the context of intact cells.

MATERIALS AND METHODS

Preparation of cells and measurement of $[Ca^{2+}]_i$ and Ca^{2+} fluxes follow the procedures described in the preceding paper. Empirical rate equations for net plasma membrane Ca^{2+} transport and for mitochondrial Ca^{2+} uptake and release were obtained by fitting equations to flux data obtained from $[Ca^{2+}]_i$ recordings that were smoothed 1–2 times with a binomial filter. The rate equations were then incorporated into a system of differential equations that was solved numerically using a 4th-order Runge-Kutta routine (Boyce and DiPrima, 1969) written in Igor Pro (Wavemetrics, Inc.). Step size was 50 ms; further reductions in step size did not noticeably alter the results. Cells were pretreated with thapsigargin (Tg) to minimize contributions from ER Ca transport, so the model does not include this organelle. The details of the model and the underlying assumptions are described in the appendix.

RESULTS

Quantitative Description of the Flux Components

We begin with analytical descriptions of the three components of the total Ca^{2+} flux. In each case, rate equations will be used that are motivated by known properties of plasma membrane and mitochondrial Ca^{2+} transport. It is then asked if the quantitative properties of the individual fluxes are sufficient to account for the kinetic properties of the $[Ca^{2+}]_i$ recovery. For this purpose, the equations may be regarded as completely em-

Figure 2. Quantitative description of $J_{Na/Ca}$ (A) Comparison between four responses elicited by 50 mM K^+ depolarizations of increasing duration from the same cell (sc0e22). Durations were (1–4, in s): 3.2, 7.5, 11.5, and 20.7. Inset shows the initial portion of the responses on an expanded time scale. (B) $[Ca^{2+}]_i$ recoveries from A are aligned in time and coded by intensity (briefest stimulus = darkest trace). (C) Time course of the net mitochondrial Ca^{2+} flux, J_{mito} calculated as the difference between the total flux in the presence and absence of FCCP (1 μM) at corresponding values of $[Ca^{2+}]_i$. (D) Time course of the integrated net mitochondrial Ca^{2+} flux ($\Delta[Ca^{2+}]_m^{(i)}$) as a measure of changes in mitochondrial Ca concentration from its resting level. $\Delta[Ca^{2+}]_m^{(i)}(t)$ rises during the initial rapid phase of recovery and then declines more slowly with a half time that increases with stimulus duration. Inset shows the relationship between $\Delta[Ca^{2+}]_m^{(i)}$ just after repolarization and stimulus duration for this cell (squares). Dashed trace shows best fit line for the last three points (slope: 71 nM/s, y-intercept: −7 nM). Results from two other cells are also shown (circles, triangles). (E) Time course of $J_{Na/Ca}$ showing the initial increase during the rapid phase of recovery and the subsequent decline that parallels the slow plateau phase of the $[Ca^{2+}]_i$ recovery. Peak $J_{Na/Ca}$ increases sublinearly with stimulus duration. $J_{Na/Ca}$ was calculated as the component of the total flux during the recovery that was sensitive to CGP (4 μM). (F) Plot of $J_{Na/Ca}$ versus $\Delta[Ca^{2+}]_m^{(i)}(t)$ for each of the recoveries along with a fit (smooth curve) based on Eq. 7 with A = −34.8 nM/s, B = 615 nM, and C = 0.03. See text for description of parameters.

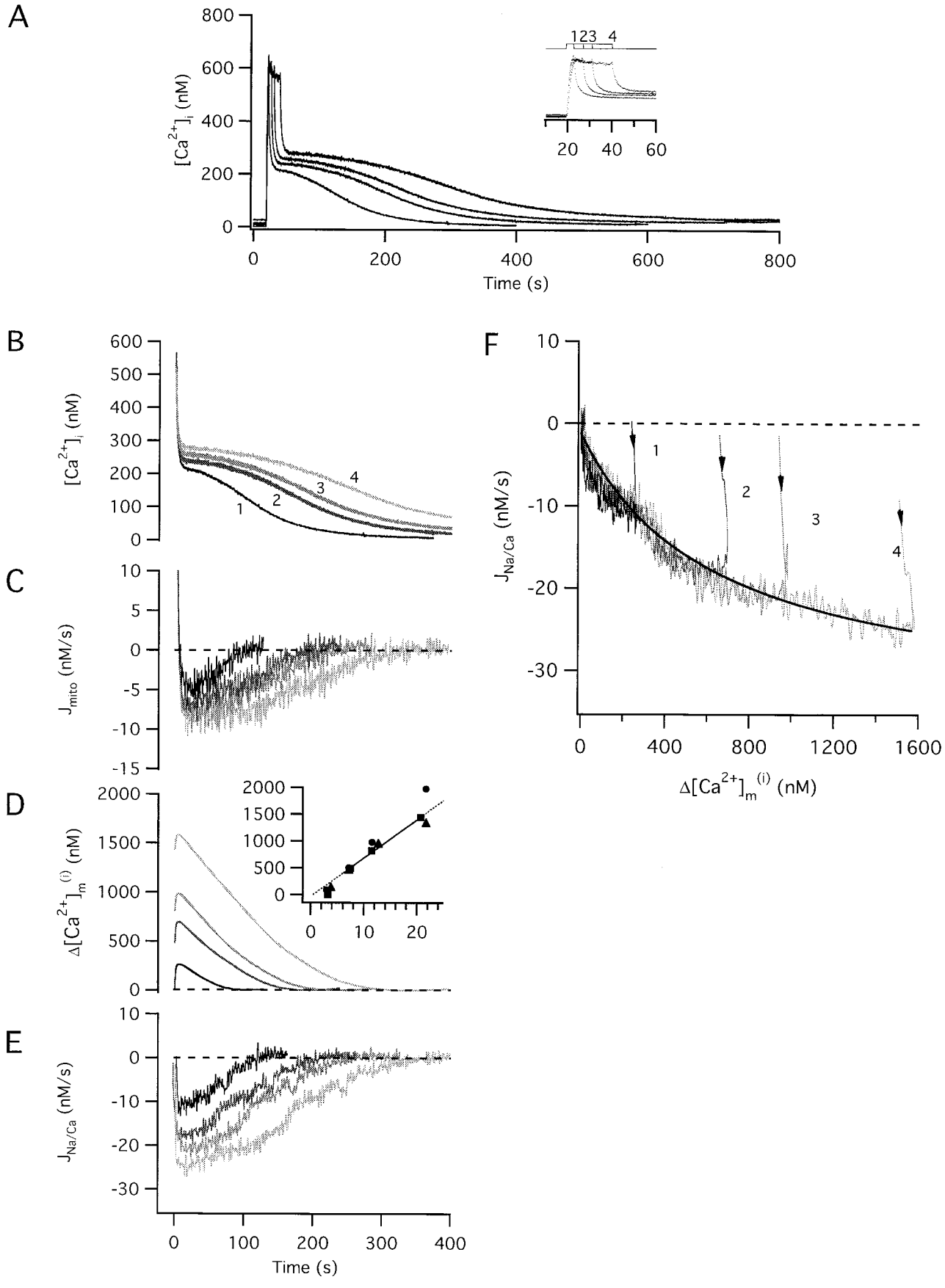
A
800
600
400
200
0
$[Ca^{2+}]_i$ (nM)
0
200
400
600
800
Time (s)
1 2 3 4
20
40
60
B
600
500
400
300
200
100
0
$[Ca^{2+}]_i$ (nM)
1
2
3
4
C
10
5
0
-5
-10
-15
J_{mito} (nM/s)
D
2000
1500
1000
500
0
$\Delta[Ca^{2+}]_m^{(i)}$ (nM)
0
10
20
E
10
0
-10
-20
-30
$J_{Na/Ca}$ (nM/s)
0
100
200
300
400
Time (s)
F
10
0
-10
-20
-30
$J_{Na/Ca}$ (nM/s)
1
2
3
4
0
400
800
1200
1600
$\Delta[Ca^{2+}]_m^{(i)}$ (nM)

pirical. However, in the Discussion, the equations and parameters describing mitochondrial Ca^{2+} transport will be considered in light of information obtained from previous studies of isolated organelles.

The $[Ca^{2+}]_i$ -dependent Fluxes: J_{pm} and J_{uni}

Fig. 1 A shows how the rate of net Ca^{2+} extrusion across the plasma membrane (J_{pm}) depends on $[Ca^{2+}]_i$ during the recovery after high K^+ depolarization, averaged over 10 cells (solid symbols). The smooth curve is a plot of Eq. 1 (see appendix) that describes the net flux generated by a linear leak operating in parallel with a saturable extrusion system. According to this equation, J_{pm} increases monotonically with $[Ca^{2+}]_i$, crossing zero at a (stable) resting level (50 nM). Eq. 1 regards J_{pm} as an instantaneous function of $[Ca^{2+}]_i$, conforming with the observed properties of this flux (see Figure 2 B of preceding study). While there is evidence for distinct components of J_{pm} that are differentially sensitive to extracellular Na^+ and La^{3+} (Friel, D.D., unpublished observations), Eq. 1 lumps together all energetically uphill Ca^{2+} transport into a single equation and should therefore be regarded as an empirical description of the measured flux. Clearly, the $[Ca^{2+}]_i$ dependence of J_{pm} is adequately described by Eq. 1 for $[Ca^{2+}]_i$ up to 800 nM. Similar results were obtained from three cells studied under voltage clamp (open symbols).

Fig. 1 B shows the $[Ca^{2+}]_i$ dependence of J_{uni} based on collected results from three cells studied under voltage clamp (open symbols). J_{uni} increases steeply and monotonically with $[Ca^{2+}]_i$ in a manner that can be described by a modified sigmoidal function of $[Ca^{2+}]_i$ (Eq. 2). According to this equation, J_{uni} depends on $[Ca^{2+}]_i$ but not $[Ca^{2+}]_m$, consistent with the finding that J_{uni} exhibits the same $[Ca^{2+}]_i$ dependence after stimuli that are expected to produce very different mitochondrial Ca^{2+} loads (see Figure 7, D and E, of preceding study). There is no indication that J_{uni} saturates over this $[Ca^{2+}]_i$ range, so no attempt was made to estimate a limiting slope ($k_{max,uni}$) or a $[Ca^{2+}]_i$ level where activation is half-maximal ($EC_{50,uni}$). However, Hill plot analysis provides an estimate of the Hill coefficient ($n_{uni} = 1.93 \pm 0.18$) that is quite insensitive to these parameters (Gunter and Gunter, 1994; see also Scarpa and Graziotti, 1973). The smooth curve shows the result of fitting Eq. 2 to the flux data with $EC_{50,uni}$ held at 10 μM (Gunter and Pfeiffer, 1990) and $n_{uni} = 2$, yielding $k_{max,uni} = 75.9$. With the same parameters, Eq. 2 also provides a good description of mean J_{uni} from 10 cells measured after high K^+ depolarization (solid symbols).

Ca^{2+} Release via the Mitochondrial Na^+/Ca^{2+} Exchanger

In the preceding study, it was shown that $J_{Na/Ca}$ exhibits an apparent U-shaped dependence on $[Ca^{2+}]_i$. Although $J_{Na/Ca}$ varies with $[Ca^{2+}]_i$, it is not clear that $J_{Na/Ca}$ actually depends on $[Ca^{2+}]_i$ (i.e., is a function of $[Ca^{2+}]_i$). Previous studies of isolated mitochondria have shown that with constant extramitochondrial Na^+ and Ca^{2+} concentrations, the rate of Ca^{2+} release via the Na^+/Ca^{2+} exchanger is a saturable function of the intramitochondrial free Ca concentration ($[Ca^{2+}]_m$; Wingrove and Gunter, 1986). To examine the dependence of $J_{Na/Ca}$ on intramitochondrial Ca levels, cells were depolarized for increasing periods of time to produce graded mitochondrial Ca^{2+} loads, and the components of the net mitochondrial Ca^{2+} flux during the subsequent recoveries were compared. Specifically, it was asked if $J_{Na/Ca}$ increases saturably with the depolarization-evoked mitochondrial Ca load.

Fig. 2 A shows $[Ca^{2+}]_i$ responses from an exemplar cell elicited by four 50 mM K^+ depolarizations of different duration. While the rise in $[Ca^{2+}]_i$ during the depolarizations and the initial recovery after repolarization were similar in each case (see inset), the subsequent phases of recovery depended strongly on stimulus duration. In particular, the slow plateau phase became longer as the duration of the preceding depolarization was increased, as described previously (Friel and Tsien, 1994). For example, the time required for $[Ca^{2+}]_i$ to fall below 25% of its value at the instant of repolarization increased from 79 to 256 s as the depolarization length increased from 3.3 to 20.7 s. There was also a small increase in the plateau level (see Fig. 2, A and B). B shows the recoveries from A aligned in time. Beneath the $[Ca^{2+}]_i$ records are time plots of the net mitochondrial Ca^{2+} flux (J_{mito}; see Fig. 2 C), integrated J_{mito} ($\Delta[Ca^{2+}]_m^{(i)}(t)$, D), and the Na^+/Ca^{2+} exchanger flux ($J_{Na/Ca}$, E). As discussed in the preceding study, $\Delta[Ca^{2+}]_m^{(i)}(t)$ provides a measure of the mitochondrial Ca^{2+} concentration at time t relative to its basal value, referred to the effective cytosolic volume. For each stimulus duration, the initial rapid decline in $[Ca^{2+}]_i$ is coincident with a large outward net mitochondrial Ca^{2+} flux (Fig. 2 C), an increase in mitochondrial Ca concentration (D) and an increase in the magnitude of $J_{Na/Ca}$ (E). In contrast, the plateau phase of recovery is associated with net mitochondrial Ca^{2+} release, a decline in mitochondrial Ca concentration, and a nearly constant inward flux via the Na^+/Ca^{2+} exchanger, each of which becomes more prolonged as the stimulus length is increased. Note that the initial value of $\Delta[Ca^{2+}]_m^{(i)}$ (i.e., the value at the end of the depolarization) is proportional to stimulus duration when the stimulus lasts at least 7.5 s (Fig. 2 D, inset). Using the measured ratio of mitochondrial and cytosolic volumes (0.1) and the estimated ratio of total and free cytosolic Ca concentration in sympathetic neurons (~200; Friel, D.D., and S.B. Andrews, unpublished observations), the proportionality constant (71 nM/s) converts to (71)(200/0.1) = 142 μM/s, in

reasonable agreement with the rate at which total mitochondrial Ca concentration rises during 50 mM K^+ depolarization in these cells as determined from electron probe microanalysis (184 μM/s; Pivovarova et al., 1999).

Importantly, J_{mito} and its inward component $J_{Na/Ca}$ are both limited as the stimulus duration increases. For example, increasing the stimulus length from 11.5 to 20.7 s nearly doubles the mitochondrial Ca load, but has relatively little effect on the peak magnitude of $J_{Na/Ca}$ (Fig. 2, compare D with E). Saturation of $J_{Na/Ca}$ can be seen more clearly by plotting $J_{Na/Ca}$ versus $\Delta[Ca^{2+}]_m^{(i)}$ during the recovery for each stimulus duration (F). In each case, $J_{Na/Ca}$ increases saturably with $\Delta[Ca^{2+}]_m^{(i)}$ in a manner that is described by Eq. 7 over most of the $\Delta[Ca^{2+}]_m^{(i)}$ range (see smooth curve). This equation, which assumes that $J_{Na/Ca}$ depends on intramitochondrial Ca^{2+} concentration but not $[Ca^{2+}]_i$, provides a simple description of the measured flux over all but the initial phase of recovery. Estimating the ratio of mitochondrial and cytoplasmic effective volumes (γ) as 2 (see previous study) gives $\Delta[Ca^{2+}]_m = \Delta[Ca^{2+}]_m^{(i)}/2$ (Eq. 4), $V_{max,Na/Ca} = -34.8$ nM/s, $EC_{50,Na/Ca} = 307.5$ nM and $[Ca^{2+}]_m(\infty) = 9.2$ nM. Results from two other cells were similar except that $V_{max,Na/Ca}$ was somewhat larger (~ -75 nM/s).

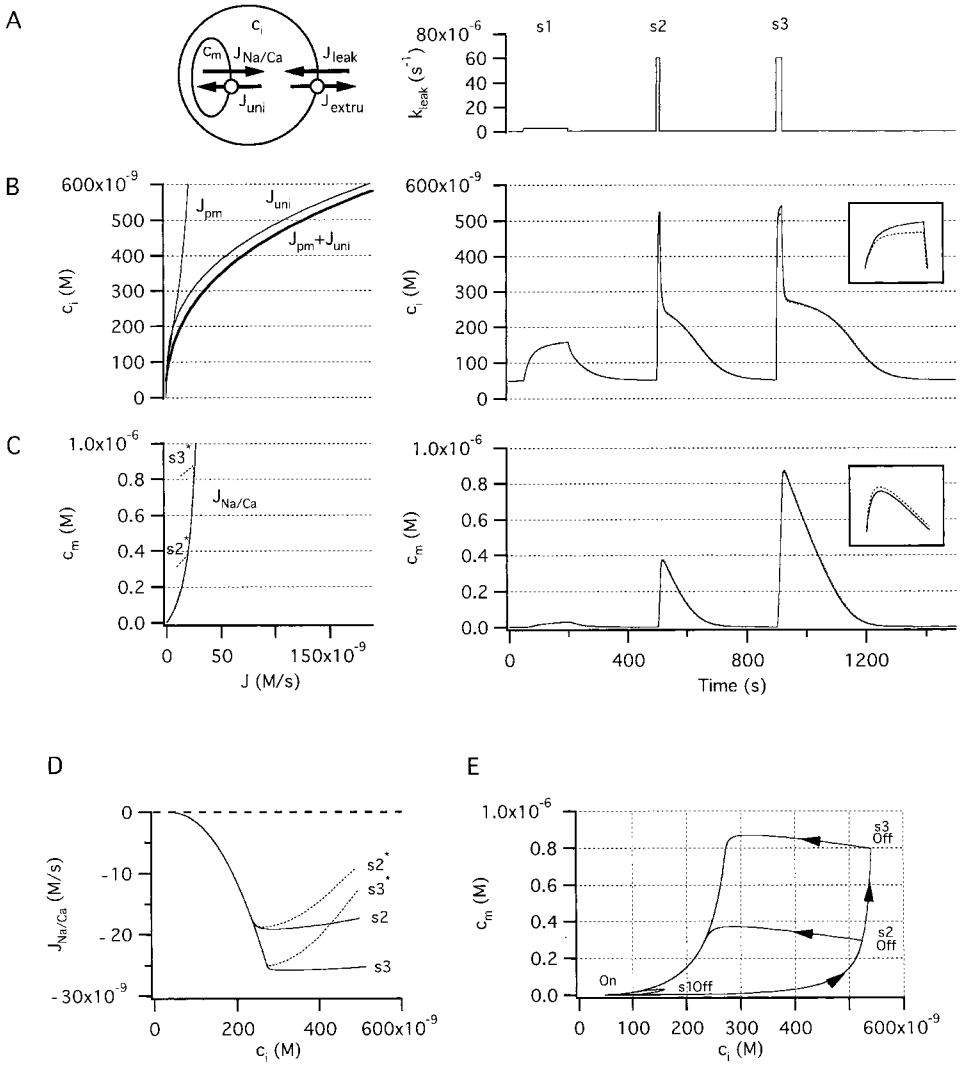

Figure 3. Simulated changes in cytosolic and mitochondrial Ca^{2+} concentration during and after stimulated Ca entry. (A, left) Schematic of the model used in the simulations indicating compartments (with Ca^{2+} concentration c_i and c_m) and pathways for Ca^{2+} movement between compartments. The net plasma membrane Ca^{2+} flux, J_{pm} is the sum of J_{leak} and J_{extru}, and the net mitochondrial Ca^{2+} flux is the sum of J_{uni} and $J_{Na/Ca}$. (Right) Ca^{2+} entry was stimulated by increasing the plasma membrane leak rate constant (k_{leak}). (B, left) c_i-dependent components of the total Ca^{2+} flux: J_{pm}, J_{uni} and $J_{pm} + J_{uni}$. Note that J_{pm} is calculated using the basal Ca^{2+} entry rate constant and therefore does not apply during stimulation. (Right) Simulated changes in c_i during and after each stimulus. Solid curves show simulated c_i values in the case where $J_{Na/Ca}$ depends only on c_m (Eq. 17), dotted curves illustrate the case where $J_{Na/Ca}$ depends on both c_m and c_i (Eq. 19). Inset shows on an expanded scale the small effect of including the c_i-dependent inhibitory factor in the definition of $J_{Na/Ca}$; inset represents a 100 nM range of c_i around the peak of the response to stimulus s3. (C, left) $J_{Na/Ca}$ and its dependence on c_m according to Eq. 17 (solid trace) or on c_m and c_i according to Eq. 19 (dotted trace). (Right) Simulated changes in c_m during and after each stimulus; solid and dotted curves as in B (right). The weak stimulus (s1) elicits a small c_i increase and therefore only activates J_{uni} weakly so that c_m undergoes a small rise. The larger stimuli (s2, s3) raise c_i sufficiently to activate J_{uni} strongly and elevate c_m to a level that depends on stimulus duration. Including the inhibitory term in the definition of $J_{Na/Ca}$ has little effect on the time courses of c_i and c_m (compare solid and dotted traces). (D) Variation of $J_{Na/Ca}$ with c_i during the recovery after s2 and s3 for comparison with the experimentally observed $[Ca^{2+}]_i$ dependence of $J_{Na/Ca}$. (E) Plot of c_m vs c_i for each of the responses illustrated in B and C (right). Unless indicated otherwise, parameter values in this and the following figures are: $k_{leak} = 3.7 \times 10^{-7}$ s^{-1}, $V_{max,extru} = 28.3$ nM/s, $EC_{50,extru} = 378.8$ nM, $n_{extru} = 1.8$, $k_{max,uni} = 80$ s^{-1}, $EC_{50,uni} = 10$ μM, $n_{uni} = 2$, $V_{max,Na/Ca} = -35$ nM/s, $EC_{50,Na/Ca} = 307$ nM, $c_o = 0.002$ and $\gamma = 2$. Parameters describing inhibition of $J_{Na/Ca}$ are $n_{inhib} = 6$ and $K_{inhib} = 500$ nM.

While the rate of mitochondrial Ca^{2+} release is described quite well by Eq. 7 during most of the recovery, it deviates systematically from this description during the initial phase when $[Ca^{2+}]_i$ highest. During this phase, the rapid decline in $[Ca^{2+}]_i$ is accompanied by a similarly rapid rise in $J_{Na/Ca}$ (Fig. 2, E and F arrows). The basis for this deviation, which is relevant to the apparent U-shaped $[Ca^{2+}]_i$ dependence of $J_{Na/Ca}$ (see preceding study, Figures 7 and 8) is not certain. However, previous studies have shown that the mitochondrial Na^+/Ca^{2+} exchanger is inhibited by extramitochondrial Ca^{2+} (Hayat and Crompton, 1982). A modified rate law that includes $[Ca^{2+}]_i$-dependent inhibition of the exchanger at high $[Ca^{2+}]_i$ (Eq. 8) provides a reasonable description of the results during the entire recovery (not shown). However, it will be shown below that the observed attenuation of $J_{Na/Ca}$ at high $[Ca^{2+}]_i$ is not expected to influence recovery kinetics very much since under these conditions J_{uni} is the dominant component of the mitochondrial Ca^{2+} flux and $J_{Na/Ca}$ represents only a small fraction of the total flux.

Below, we examine the behavior of a model in which plasma membrane Ca^{2+} transport is described by Eq. 1, mitochondrial Ca^{2+} uptake is described by Eq. 2, and mitochondrial Ca^{2+} release is described by Eqs. 7 or 8, with parameter values obtained directly from the experimental data presented above. It is found that the model accounts very well for most of the features of $[Ca^{2+}]_i$ recovery kinetics in sympathetic neurons.

Simulated Changes in Intracellular Ca^{2+} Concentration Induced by Ca^{2+} Entry

To determine if the quantitative properties of J_{pm}, J_{uni}, and $J_{Na/Ca}$ are sufficient to account for $[Ca^{2+}]_i$ dynamics during the recovery, the rate equations described above were taken as the flux definitions in a previous model of Ca dynamics in sympathetic neurons (Friel and Tsien, 1994). In this model, mitochondria contain Ca^{2+} at concentration c_m and are exposed to cytosolic Ca^{2+} at concentration c_i (Fig. 3 A, left). It is assumed that c_i is spatially uniform within the cytosol, which is a reasonably accurate description of $[Ca^{2+}]_i$ during the recovery since $[Ca^{2+}]_i$ gradients dissipate rapidly ($\sim$1 s) after repolarization (Hernandez-Cruz et al., 1990; Hua et al., 1993). With regard to the spatial distribution of intramitochondrial Ca, reversible formation of Ca- and P-rich

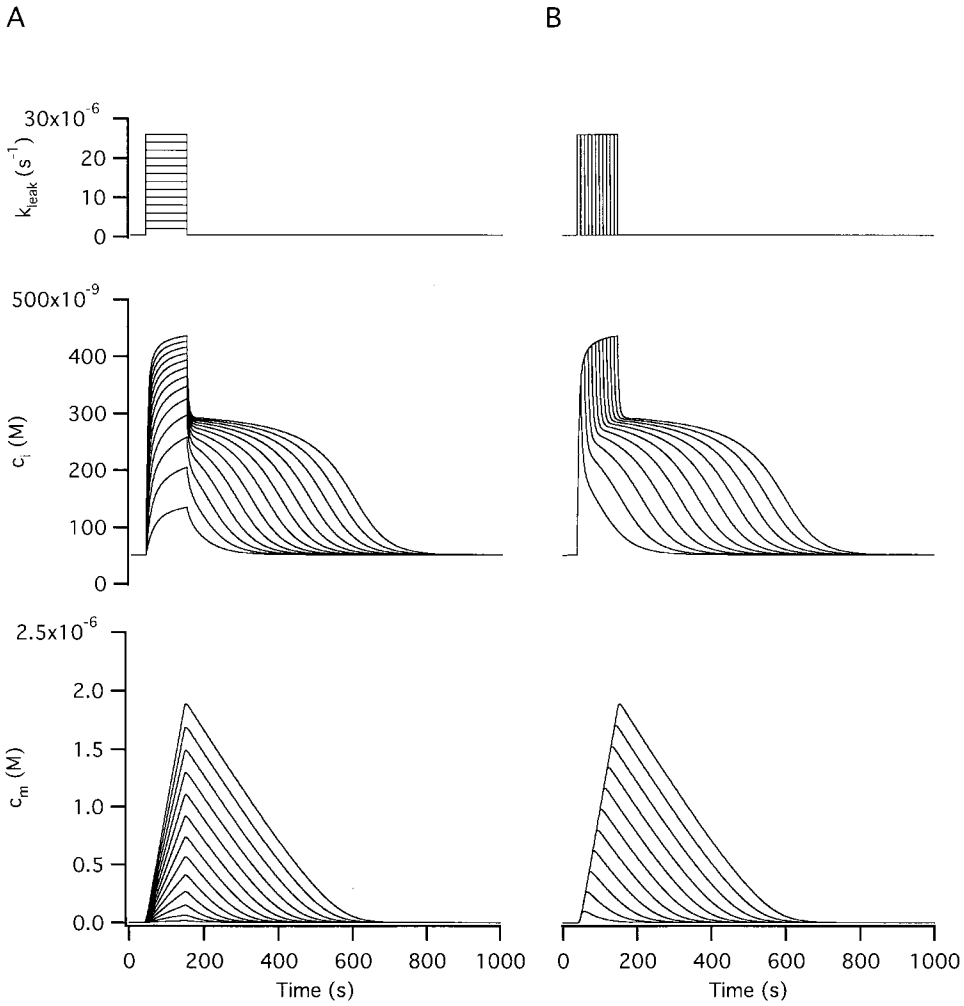

Figure 4. Simulated responses to stimuli of graded intensity and duration. (A) Changes in c_i and c_m elicited by 110 s stimuli of graded intensity. During weak stimulation, c_i and c_m approach new elevated steady state values, while during the stronger stimuli c_i approaches a steady elevated level and c_m rises linearly with time. After the stronger stimuli, c_i falls to a plateau level and then recovers with a time course much like that observed experimentally. (B) Changes in c_i and c_m elicited by stimuli of fixed magnitude equal to the strongest stimulus in A but of variable duration. With increasing stimulus duration, c_i approaches a steady elevated level where c_m increases in proportion to stimulus length (compare with Fig. 2 D, inset). After the stimulus ends, the rapid decline in c_i is accompanied by a rise in c_m, and during the plateau phase c_m falls at a nearly constant rate, causing c_i to remain elevated at a nearly constant level that increases saturably with mitochondrial Ca^{2+} load.

intramitochondrial inclusions has been observed under these conditions of stimulation (Pivovarova et al., 1999), but there is no evidence that the distribution of intramitochondrial free Ca outside the inclusions is spatially heterogeneous. Therefore, it will be assumed for simplicity that c_m is spatially uniform within the mitochondrial compartment.

In the model, Ca^{2+} extrusion across the plasma membrane occurs at rate J_{extru} and passive Ca^{2+} entry occurs at rate J_{leak}. These two fluxes define the net Ca^{2+} flux across the plasma membrane (J_{pm}). Mitochondrial Ca^{2+} uptake is described by J_{uni} and Ca^{2+} release is described by $J_{Na/Ca}$; these two fluxes define the net mitochondrial Ca^{2+} flux. Since J_{pm} and J_{uni} are both defined by c_i, they are plotted together against c_i in B (left) along with their sum (thick trace). $J_{Na/Ca}$ is plotted both versus c_m (Fig. 3 C, left, shown as a positive flux for simplicity) and versus c_i (D) for comparison with the results in the preceding study (e.g., Figures 7 and 8); solid traces describe the case where $J_{Na/Ca}$ depends only on c_m and dotted traces illustrate the case where this flux depends on both c_m and c_i.

Simulated changes in c_i and c_m after step increases in the rate constant of Ca^{2+} entry (Fig. 3 A, right) are plotted in B and C (right); note that the c_i- and c_m-dependent fluxes can be read from the corresponding plots at left. During a small stimulus (s1) that elevates c_i to a low level ($\sim$160 nM, Fig. 3 B, right), J_{uni} is only weakly activated (B, left) so that c_m increases to a low level ($<$50 nM, C right). In this case, when the stimulus ends, the net mitochondrial Ca^{2+} flux is small compared with J_{pm} so the c_i recovery is dominated by Ca^{2+} extrusion across the plasma membrane, accounting for the simple recovery kinetics. With a stronger stimulus (s2) that raises c_i to a higher level, J_{uni} is activated more strongly, causing robust Ca^{2+} accumulation and a rapid rise in c_m.

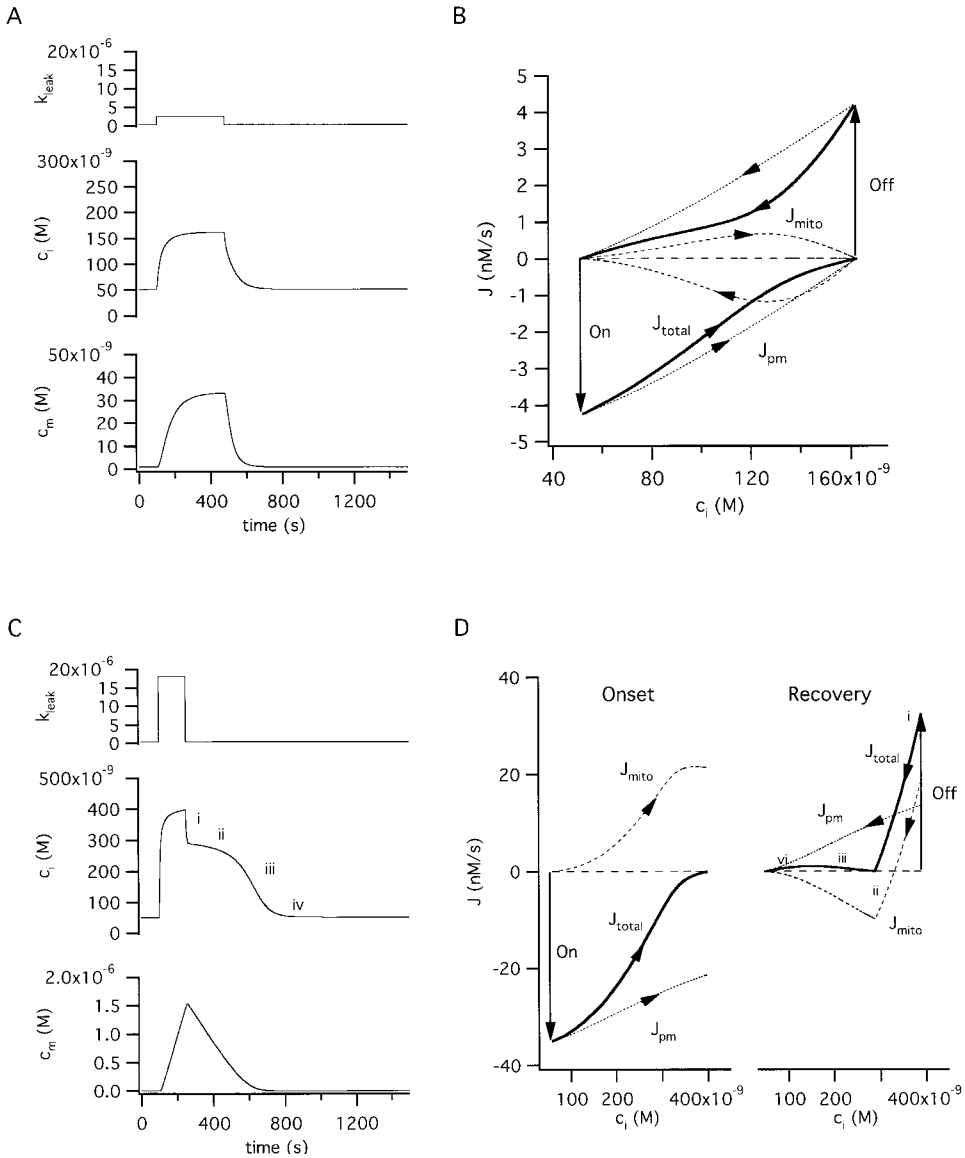

Figure 5. Comparison between responses to weak and strong stimulation (A) Simulated c_i and c_m responses elicited by a weak stimulus that raises c_i and c_m to new steady-state levels. (B) Ca^{2+} fluxes responsible for changes in c_i and c_m in A. The total cytosolic Ca^{2+} flux (J_{total}) is shown (thick trace) along with its components J_{pm} (dotted trace) and J_{mito} (dashed trace). The downward arrow (On) indicates when the stimulus begins, and the upward Off arrow indicates when the stimulus ends. Inward fluxes are negative and outward fluxes are positive. (C) Simulated c_i and c_m responses elicited by a strong stimulus. (D) The Ca^{2+} fluxes underlying the changes in c_i and c_m are shown separately in C during the onset (left) and the recovery (right). As with the measured fluxes J_{total} and $J_{mito,}$ the simulated fluxes during the recovery are biphasic and exhibit minima during the plateau phase. See text for details.

Due to its steep c_i dependence, J_{uni} is nearly four times larger than $J_{Na/Ca}$ at the highest c_i levels achieved during stimulation, setting the stage for continuous mitochondrial Ca^{2+} accumulation. When this stimulus ends, continued Ca^{2+} accumulation contributes to a rapid rise in c_m and decline in c_i (Fig. 3 E; see Fig. 5 C from Babcock et al., 1997). This decline in c_i, in turn, deactivates J_{uni} and shifts the balance from mitochondrial Ca^{2+} accumulation to net release, which initiates the slow plateau phase of recovery. Finally, as c_i approaches its resting level, net Ca^{2+} extrusion across the plasma membrane dominates. A longer stimulus (s3) raises c_i to about the same level but for a longer period of time, leading to a larger increase in c_m. As a result, the c_i recovery is even more prolonged. Overall, the recovery kinetics are very similar to those observed experimentally in terms of sensitivity to stimulus strength and duration, the four distinct phases of recovery, and the level of the plateau (Friel and Tsien, 1994; see Fig. 2 A of this study).

If the rate description of $J_{Na/Ca}$ is modified to include inhibition by c_i, $J_{Na/Ca}$ is no longer completely defined by c_m and is depressed during the initial rapid phase of recovery when c_i is high, showing an apparent U-shaped dependence on c_i like the measured flux (dotted curves $s2^*$, $s3^*$ in Fig. 3, C and D). However, the time courses of c_i and c_m are nearly unchanged (see dotted curves in B and C right, insets). The explanation is simple: $J_{Na/Ca}$ constitutes only a small fraction of the total mitochondrial Ca^{2+} flux over the c_i range where inhibition occurs, so that inhibition has little impact on the total flux. Since inhibition of $J_{Na/Ca}$ during the initial phase the recovery does not appreciably influence the dynamics of c_i or c_m, for simplicity, it will be ignored in the following, and it will be assumed that $J_{Na/Ca}$ depends only on c_m.

Responses to Stimuli of Variable Magnitude and Duration

Fig. 4 A illustrates responses to stimuli of fixed duration and increasing strength. Weak stimuli that raise c_i to low levels barely activate the uniporter so that mitochondrial Ca^{2+} accumulation is slow. Thus, when the stimulus ends, Ca^{2+} uptake and release rates are low, so the recovery kinetics depend almost entirely on Ca^{2+} extrusion across the plasma membrane. Stronger stimuli that raise c_i to higher levels increasingly activate the uniporter, causing Ca^{2+} accumulation at progressively higher rates (see Fig. 4 A, bottom). During each stimulus, c_i and the rate of mitochondrial Ca^{2+} accumulation both approach steady values, and when the stimulus ends, continued mitochondrial Ca accumulation speeds the initial c_i decline. This leads to partial deactivation of the uniporter, causing Ca^{2+} accumulation to give way to net release, which then slows the c_i recovery. As discussed in the next section, when the mitochondrial Ca^{2+} load is large, the rate of Ca^{2+} release via the Na^+/Ca^{2+} exchanger, and the rate of net mitochondrial Ca^{2+} release, are both nearly constant, causing c_i to hang up at an elevated plateau level until c_m falls and saturation of the exchanger is relieved. The c_i plateau level, defined as the c_i level where the recovery rate reaches a minimum, increases with stimulus strength and appears to approach a limiting value where c_i declines at a vanishingly slow rate (see below).

Fig. 4 B illustrates responses to stimuli of fixed magnitude and variable duration. In this case, the briefest stimulus raises c_i sufficiently to activate the uniporter, and increasing the stimulus duration increases the mitochondrial Ca^{2+} load. As the stimulus length increases, c_i approaches a steady elevated level and c_m rises linearly with time (compare with Fig. 2 D, inset). When the stimulus ends, c_i undergoes a rapid decline to a plateau level that depends on stimulus duration (compare with Fig. 2 A) and eventually recovers to basal levels.

Comparison between Simulated Responses to Weak and Strong Stimulation: Analysis of the Underlying Fluxes

Mitochondrial Ca^{2+} uptake has often been viewed as a low-affinity process that is only important when $[Ca^{2+}]_i$ rises to high levels, either in microdomains near mitochondria during physiological stimulation (Rizzuto et al., 1998), or after Ca^{2+} overload under extreme conditions (Moravec and Bond, 1992; Horikawa et al., 1998). One reason is that the EC_{50} for the uniporter is high ($\sim$10–20 μM; Gunter and Pfeiffer, 1990). How is mitochondrial Ca concentration expected to change during stimulation that raises $[Ca^{2+}]_i$ only slightly above the resting level? A simulated response to a long, weak stimulus is shown in Fig. 5 A. During the stimulus, both c_i and c_m rise to new steady state levels ($c_m < c_i$) and return to their prestimulation values after the stimulus ends. The changes in c_i and c_m can be understood by considering the underlying fluxes (Fig. 5 B). Before stimulation, there is a steady state distribution of Ca^{2+}, and the total cytosolic Ca^{2+} flux (J_{total}) and its components J_{pm} and J_{mito}, are all zero. When the stimulus begins (On arrow), J_{total} (thick trace) suddenly becomes an inward flux so that c_i rises and then gradually declines toward zero as c_i approaches a new elevated steady state level. When the stimulus ends, J_{total} suddenly becomes an outward flux (Off arrow), which causes c_i to return to its basal level. Note that during the onset, J_{pm} includes contributions from both basal and stimulated Ca^{2+} entry as well as Ca^{2+} extrusion.

The changes in J_{total} can be understood by examining the component fluxes. With the onset of stimulation, the rate of Ca^{2+} entry suddenly increases, creating an imbalance between Ca^{2+} entry and extrusion which

causes J_{pm} (dotted trace), and therefore J_{total}, to suddenly become inwardly directed (On arrow). As c_i rises, the rate of Ca^{2+} extrusion increases, eventually equaling the rate of Ca^{2+} entry, so that J_{pm} declines to zero. The rise in c_i also creates an imbalance between mitochondrial Ca^{2+} uptake and release, leading to net mitochondrial Ca^{2+} accumulation (J_{mito} positive, dashed trace) which slows the rise in c_i. As c_m rises, Ca^{2+} release eventually balances uptake and J_{mito} falls to zero. Termination of the stimulus creates a sudden imbalance between Ca^{2+} entry and extrusion which causes J_{pm} (and J_{total}) to become outward fluxes (Off arrow) so that c_i declines. As the rate of Ca^{2+} extrusion approaches the rate of entry, J_{pm} approaches zero. The decline in c_i also creates an imbalance between mitochondrial Ca^{2+} uptake and release, leading to net Ca^{2+} release (J_{mito} negative, dashed trace), which slows the c_i recovery. As c_i and c_m return to their resting levels, the rates of Ca^{2+} uptake and release both decline and J_{pm} and J_{mito} approach zero. Thus, a weak stimulus leads to a reversible transition between two steady states in which all intercompartmental net fluxes are zero.

Strong stimuli produce qualitatively different responses (Fig. 5, C and D). For clarity, the fluxes underlying the response onset and recovery are shown separately (Fig. 5 D, left and right, respectively). When the stimulus begins, J_{total} instantly becomes a large inward flux (Fig. 5 D left, thick trace, On arrow) and then declines to zero as c_i stabilizes at a new elevated level. However, in this case, J_{total} approaches zero not because the component fluxes individually fall to zero, but because the outward flux J_{mito} eventually balances the inward flux J_{pm}. This occurs when c_i is so high that J_{uni} exceeds the maximal rate of Ca^{2+} release via the Na^+/Ca^{2+} exchanger, setting the stage for continuous mitochondrial Ca^{2+} accumulation at a rate that equals the rate of net Ca^{2+} entry. When the stimulus ends, J_{total} suddenly becomes a large outward flux (Fig. 5 D right, thick trace, Off arrow) which causes c_i to fall rapidly. However, J_{total} does not decline continuously, but instead reaches a minimum and then rises again to reach a maximum before finally approaching zero. J_{total} is biphasic because it is the sum of J_{pm}, which increases montonically with c_i, and J_{mito}, which is biphasic, representing an initial phase of Ca^{2+} accumulation and a late phase of net Ca^{2+} release. The similarity between the simulated and measured fluxes during the recovery is clear (compare with Fig. 3 D in the preceding study).

The interplay between the components of the total flux explains the four phases of the c_i recovery (Fig. 5, C and D right). During phase i, both J_{mito} and J_{pm} are positive, accounting for the initial rapid c_i decline. The reduction in c_i causes partial deactivation of J_{uni} and a reduction in the rate of mitochondrial Ca^{2+} accumulation. When the rates of Ca^{2+} uptake and release are equal, J_{mito} is zero, but the decline in c_i continues because of ongoing net Ca^{2+} extrusion. Further deactivation of J_{uni} causes mitochondrial Ca^{2+} accumulation to give way to net release (phase ii) which slows the recovery. However, as c_m falls, the rate of Ca^{2+} release declines so that J_{mito} approaches zero. As a result, J_{total} rises, accounting for the accelerated recovery during phase iii. Finally, as J_{mito} approaches zero, the recovery is dominated by net Ca^{2+} extrusion across the plasma membrane (phase iv).

Simulated Effects of CGP on Responses to Weak Stimulation

In the preceding study, it was shown that despite being largely insensitive to FCCP, $[Ca^{2+}]_i$ responses elicited by weak depolarization are strongly depressed by CGP.

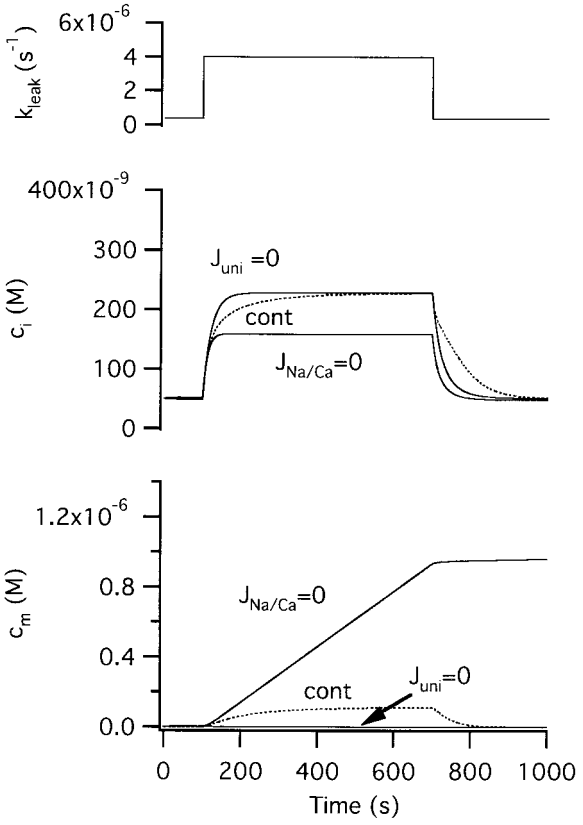

Figure 6. Simulated effects of treatment with CGP and FCCP on responses to weak depolarization. Responses to a long weak stimulus before (cont) and after setting $V_{max,Na/Ca}$ to zero to model the actions of CGP at a saturating concentration; $k_{max,uni}$ was set to zero to model the actions of FCCP. When the release pathway is inhibited ($V_{max,Na/Ca} = 0$) mitochondria accumulate Ca^{2+} continuously during stimulation so that c_i stabilizes before reaching the steady-state level observed under control conditions. This can be explained by the underlying fluxes (see Fig. 5 B) in the case where the net mitochondrial Ca^{2+} flux is given by J_{uni}. In that case, the value of c_i where J_{total} is zero is shifted to a lower value where J_{pm} is negative. If uptake in then inhibited ($k_{max,uni} = 0$), c_m does not increase in response to the stimulus and c_i changes more rapidly, and the steady-state c_i level attained during stimulation is restored to the control level.

This makes sense in light of the preceding discussion. After inhibiting mitochondrial Ca^{2+} release, weak stimuli that would otherwise lead to transient mitochondrial Ca^{2+} accumulation are expected to cause continuous accumulation and depressed $[Ca^{2+}]_i$ elevations, as in the strong stimulus regime described above. Fig. 6 shows simulated responses to a long, weak stimulus that under control conditions raises c_i to a steady state level of ~230 nM and c_m to ~100 nM. To model the actions of CGP, $V_{max,Na/Ca}$ was set to zero. In this case ($J_{Na/Ca}$ = 0), the same stimulus elicited a smaller steady rise in c_i that was accompanied by a continuous rise in c_m. $V_{max,uni}$ was then set to zero to model the additional effects of FCCP (J_{uni} = 0). This abolished the stimulus-evoked rise in c_m and speeded the elevation in c_i, reversing the simulated actions of CGP. Moreover, after inhibiting uptake, c_i rose to the same steady state level during stimulation as it did in the control. These simulations reproduce the observed effects of CGP and FCCP on steady $[Ca^{2+}]_i$ elevations elicited by weak depolarization (see Figure 9 D of the preceding study; Friel and Tsien, 1994).

The Basis for the Plateau Level and Its Relationship to the Mitochondrial Ca^{2+} Set Point

Previous studies have identified the $[Ca^{2+}]_i$ plateau level with the mitochondrial Ca^{2+} set point (Thayer and Miller, 1990) but the actual relationship between these two quantities has not been described. In the preceding study, the plateau level was defined as the c_i level where J_{total} reaches a minimum during the recovery. As shown in Fig. 5 (D, right), J_{total} reaches a minimum when the rate of mitochondrial Ca^{2+} release is nearly maximal (and J_{mito} is close to its minimal value). From the family of responses shown Fig. 4 A, it is apparent that the plateau level approaches a limiting value as the stimulus raises c_m to progressively higher levels, and that the rate of recovery at the plateau approaches zero. The basis for the plateau level and its limiting value is examined in Fig. 7. Fig. 7, B and C, show simu-

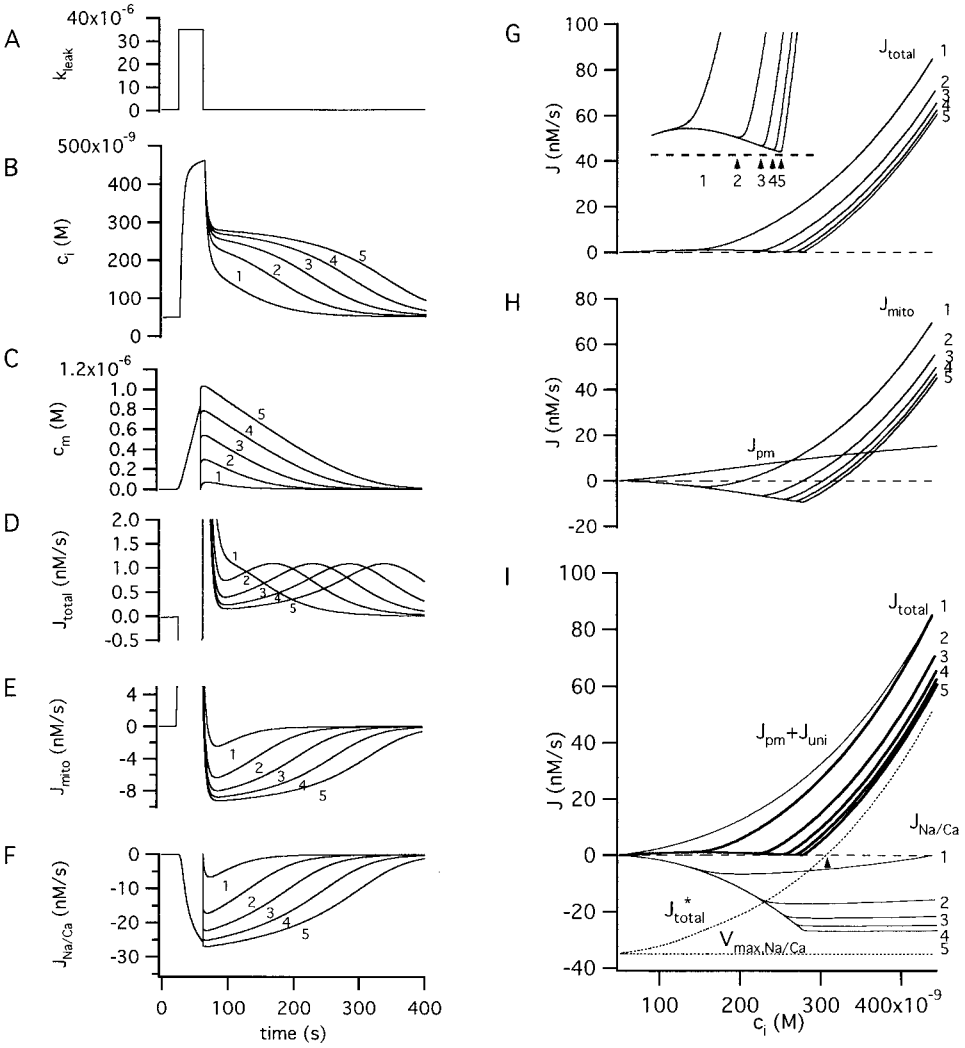

Figure 7. Basis of the Ca^{2+} plateau level and its limiting value. Simulated responses to a step increase in k_{leak} (A) showing how relaxations of c_i (B) and c_m (C) are influenced by the initial value of c_m at the beginning of the recovery. Also shown are time plots of J_{total} (D), J_{mito} (E) and $J_{Na/Ca}$ (F). (G) Plot of J_{total} versus c_i. Inset shows flux minima (arrows 2–5) on an expanded scale. There is no J_{total} minimum during recovery 1, and the minima during recoveries 2–5 occur at progressively higher c_i as the initial value of c_m is increased. (H) Plot showing the components of J_{total} (J_{mito} and J_{pm}) versus c_i during the recovery for responses 1-5. (I) Plots of J_{total} (thick traces) and an alternative set of components (J_{pm} + J_{uni}), which depends only on c_i, and $J_{Na/Ca}$ which depends on c_m (thin traces). Dotted traces show $V_{max,Na/Ca}$ and J_{total}* = (J_{pm} + J_{uni}) + $V_{max,Na/Ca}$. Note that the value of c_i where J_{total}* is zero represents a stable steady-state (see arrow). The initial value of c_m when the recovery began was 0 for trace 1 and was incremented by 250 nM for each of the successive responses (2–5). Horizontal dashed traces in G–I indicate zero net flux.

lated c_i and c_m responses elicited by the same strong stimulus (A) with the initial value of c_m set at the beginning of the recovery to different levels. Also shown are the time courses of J_{total} (D), J_{mito} (E), and $J_{Na/Ca}$ (F).

If the recovery begins with c_m equal to zero (Fig. 7 C, trace 1), c_m never reaches a very high level and the rate of net mitochondrial Ca^{2+} release is low during the entire recovery (E). In this case, J_{total} does not exhibit a minimum (Fig. 7 D) so there is no c_i plateau (B). With larger initial values of c_m (Fig. 7 C, traces 2–5), J_{total} passes through a minimum that approaches zero (D) and the c_i plateaus become increasingly flat (B). Another way to visualize how the J_{total} minimum is influenced by mitochondrial Ca^{2+} load is to plot this flux against c_i during each of the recoveries (Fig. 7 G). As shown in the inset, the magnitude of J_{total} at the minimum approaches zero, and the value of c_i where the minimum occurs approaches a limiting value. In each case, the J_{total} minimum occurs near the c_i level where J_{mito} is minimal (Fig. 7, compare G with H) and the magnitude of $J_{Na/Ca}$ is maximal.

The basis for the plateau and its limiting level finally becomes clear when J_{total} for each of the five recoveries (Fig. 7 I, thick traces 1–5) is separated into its c_i-dependent component ($J_{pm} + J_{uni}$) and the remaining (c_m-dependent) component, $J_{Na/Ca}$. During each recovery, ($J_{pm} + J_{uni}$) (thin trace) declines montonically with a stereotyped c_i dependence. In contrast, the rate of Ca^{2+} release ascends to a peak during phase i of the recovery as c_i falls and c_m rises, and then descends as c_m declines, having an initial value that depends on c_m (Fig. 7, thin traces 1–5); the peak is sharper if the rate equation for $J_{Na/Ca}$ includes inhibition by cytosolic Ca^{2+} (see Fig. 3 D). In terms of the model, it is the $J_{Na/Ca}$ peak that is responsible for the J_{mito} and J_{total} minima, and therefore the c_i plateau. As the initial mitochondrial Ca^{2+} load increases, the release pathway nears saturation, the magnitude of $J_{Na/Ca}$ during the initial phase of recovery approaches $V_{max,Na/Ca}$ (horizontal dotted line) and the plateau level approaches a limiting value. This is the (stable) steady state value of c_i that would be reached if c_m were clamped at such a high value that the rate of Ca^{2+} release is maximal ($J_{Na/Ca} \sim V_{max,Na/Ca}$) and c_i were allowed to relax from its initial value at the end of the stimulus. In this case, J_{total} would be described by $J_{total}^* = (J_{pm} + J_{uni}) + V_{max,Na/Ca}$ (dotted curve), which crosses the zero-net flux axis at the limiting plateau level (Fig. 7 I, up arrow). Here, the outward flux ($J_{pm} + J_{uni}$) and the inward flux $V_{max,Na/Ca}$ are in balance. Of course, if c_m is free to change, the limiting plateau level is never attained because the mitochondrial pool is finite and c_m and $J_{Na/Ca}$ ultimately decline.

Therefore, the limiting plateau level depends not only on the properties of mitochondrial Ca^{2+} release but also on uptake (Nicholls, 1985) and on plasma membrane Ca^{2+} transport. Increasing the release rate, either by increasing mitochondrial Ca^{2+} load or raising $V_{max,Na/Ca}$, would shift the plateau level to higher c_i, while increasing either J_{uni} or J_{pm} would shift it to lower values (Fig. 7 I). This illustrates how the effect of mito-

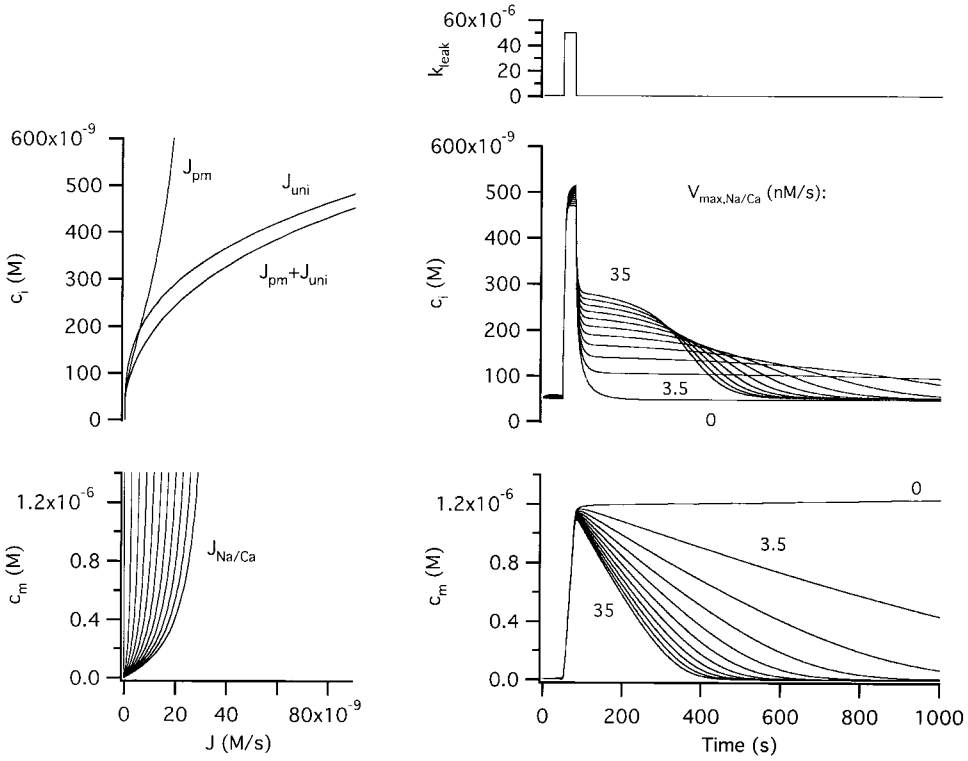

Figure 8. Simulated effect of graded inhibition of the Na^+/Ca^{2+} exchanger. Family of c_i and c_m responses simulated using a fixed stimulus but different values of $V_{max,Na/Ca}$ to examine the effect of partial inhibition of the Na^+/Ca^{2+} exchanger on response kinetics. When $V_{max,Na/Ca}$ is 35 nM/s, c_m declines rapidly during the recovery, the c_i plateau is high and the duration of the slow phase of recovery is brief. Reducing $V_{max,Na/Ca}$ stepwise progressively slows the c_m recovery and lowers and prolongs the c_i plateau. When $V_{max,Na/Ca}$ is zero, there is no plateau phase of the c_i recovery and c_m remains high; the slow increase in c_m represents Ca^{2+} uptake via the (unopposed) J_{uni} pathway.

chondrial Ca^{2+} transport on intracellular Ca^{2+} dynamics depends not only on properties of the Ca^{2+} uptake and release pathways but also on the cellular context in which they operate.

Graded Inhibition of $J_{Na/Ca}$: Comparison with the Actions of CGP

It has been proposed that the $[Ca^{2+}]_i$ plateau is caused by mitochondrial Ca^{2+} release via the Na^+/Ca^{2+} exchanger (Thayer and Miller, 1990). However, it was shown above that according to the model, the limiting c_i plateau level is influenced by both mitochondrial and nonmitochondrial Ca^{2+} transport. To examine how the Na^+/Ca^{2+} exchanger influences c_i recovery kinetics, simulations were carried out after reducing $V_{max,Na/Ca}$ stepwise (Fig. 8). This yielded a family of c_i responses whose recoveries show a similar initial rapid phase but progressively lower and longer plateaus. When $V_{max,Na/Ca}$ is large (e.g., 35 nM/s), c_m declines at a rapid, nearly constant rate during the plateau phase, causing c_i to hang up at an elevated level just below 300 nM until c_m falls and saturation of the release pathway is relieved. When $V_{max,Na/Ca}$ is small (e.g., 3.5 nM/s), c_m declines at a much slower rate, leading to a lower and more prolonged plateau that appears as a slow c_i tail like that seen during recoveries in the presence of CGP at nearly saturating concentrations (see preceding study, Figure 4 A). In each case, it is as if during the plateau phase Ca^{2+} was injected into the cytoplasm at a nearly constant rate, causing c_i to be elevated to an extent that varies directly with the rate of injection. However, since the exchanger is not completely saturated and the mitochondrial pool is exhaustible, c_i is not a constant during the plateau phase but instead declines. The response onset is less sensitive to changes in $V_{max,Na/Ca}$ than the recovery because $J_{Na/Ca}$ constitutes a smaller fraction of the total net Ca^{2+} flux when c_i is high. The simulated responses can be compared with responses elicited during treatment with CGP at subsaturating concentrations (see Figure 4 B of accompanying study).

Effect of Graded Changes in $V_{max,uni}$: Comparison with the Effects of FCCP

It was shown above that disabling mitochondrial Ca^{2+} accumulation only slightly modifies responses to weak stimuli, in agreement with the observed effects of FCCP (see Fig. 6). In that simulation, Ca^{2+} accumulation was inhibited by setting $k_{max,uni}$ to zero. Fig. 9 illustrates how graded changes in $k_{max,uni}$ influence responses to strong stimuli. When uptake is completely inhibited ($k_{max,uni}$ = 0) c_i responses resemble those seen in the presence of FCCP. As $k_{max,uni}$ is increased, mitochondrial Ca^{2+} accumulation proceeds at progressively higher rates so that c_m rises more rapidly and reaches higher levels by the end of the stimulus. This is accompanied by a slower and smaller rise in c_i during the stimulus, and a modified recovery marked by a faster phase i and a slower phase ii with lower plateau level. When $k_{max,uni} = 80\ s^{-1}$,

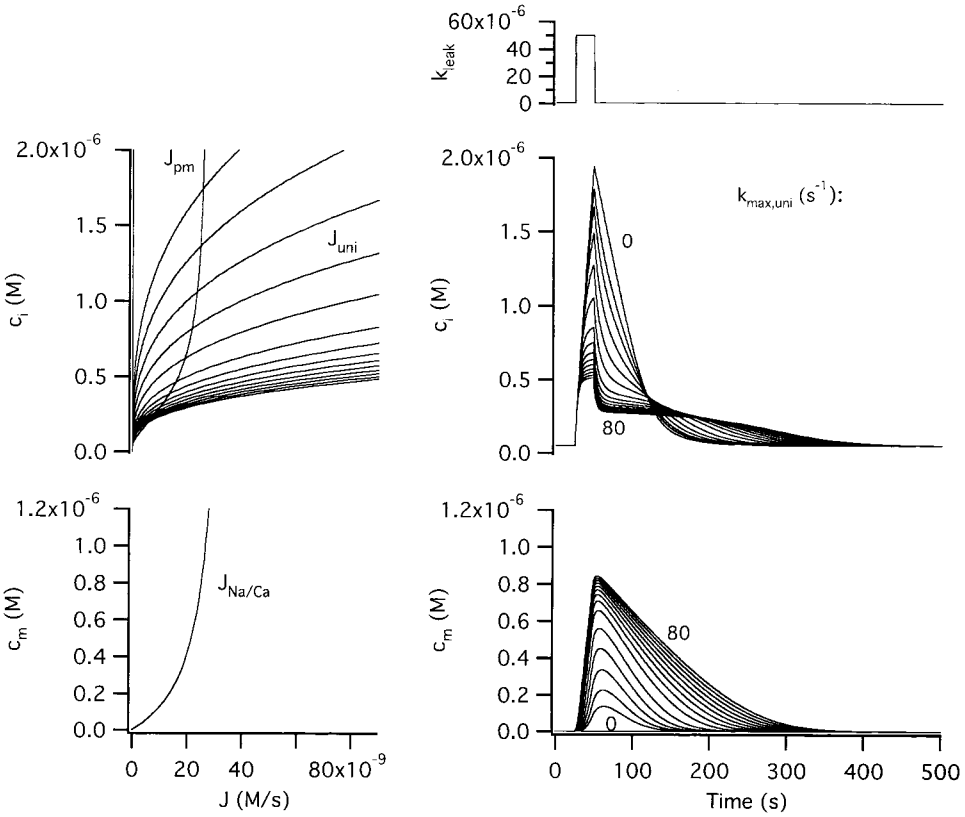

Figure 9. Sensitivity of stimulus-evoked changes in c_i and c_m to the strength of the Ca^{2+} uptake pathway. Family of responses simulated with increasing values of $k_{max,uni}$ to illustrate how the rate of Ca^{2+} uptake via the uniporter influences c_i and c_m dynamics. $k_{max,uni}$ was increased from zero to 0.5, 1, 2, 4, and 8 s^{-1} and thereafter in increments of 8 s^{-1} up to 80 s^{-1}. Raising $k_{max,uni}$ increases the rate of Ca^{2+} accumulation during stimulation so that c_m rises more rapidly and c_i rises more slowly to approach a lower steady level. After the stimulus ends, the initial rapid decline in c_i becomes faster, the plateau is lower and the overall recovery is prolonged. See text for explanation.

c_i responses resemble $[Ca^{2+}]_i$ responses elicited by depolarization in the absence of FCCP.

The effects of increasing $k_{max,uni}$ can be explained as follows. The plateau level is lowered because the maximal rate of net mitochondrial Ca^{2+} release during the recovery is reduced owing to stronger Ca^{2+} uptake at each value of c_i; the lower rate of net Ca^{2+} release also causes the recoveries to be more prolonged. Net mitochondrial Ca^{2+} release is slower in spite of increased mitochondrial Ca^{2+} loads, which by themselves would tend to increase $J_{Na/Ca}$. This is because the release pathway is nearly saturated, and the rate of release is low compared with uptake over this range of concentrations.

Effect of Graded Changes in Ca^{2+} Extrusion Rate: Relationship between the Plateau Level and the Mitochondrial Ca^{2+} Set Point

The mitochondrial set point concept provides an elegant explanation of the ability of isolated mitochondria to maintain the extramitochondrial Ca concentration at a fixed value when the intramitochondrial Ca^{2+} concentration is high. As described previously, the basis of the set point lies in the relationship between mitochondrial Ca^{2+} uptake and release pathways: if intramitochondrial Ca^{2+} concentration is high enough that the rate of release is constant, then uptake by the uniporter will maintain the extramitochondrial steady state Ca^{2+} concentration at a fixed level (Nicholls and Akerman, 1982; Crompton, 1985; Hansford, 1985). While this applies to isolated mitochondria in a closed system, it does not adequately describe mitochondrial Ca^{2+} transport in intact cells. It was shown above that the limiting plateau level, when the mitochondrial Ca^{2+} load is large, depends not only on mitochondrial Ca^{2+} transport but also on the rate of Ca^{2+} extrusion. Simulations shown in Fig. 10 illustrate how the plateau level is influenced by the rate of Ca^{2+} extrusion under conditions where the Na^+/Ca^{2+} is not completely saturated. As $V_{max,extru}$ is lowered, c_i declines more slowly, which increases the activity of the uniporter and thereby lowers the rate of net mitochondrial Ca^{2+} release. These two factors elevate and prolong the plateau. In the limiting case where $V_{max,extru}$ is zero and the plasma membrane is impermeable to Ca^{2+}, the model describes the properties of Ca^{2+} transport by isolated mitochondria in a closed system; in this case, c_i ultimately stabilizes at the set point.

Simulated Responses to Brief and Long Periodic Stimulus Trains

It was shown previously that after brief trains of stimulated action potentials that elevate $[Ca^{2+}]_i$ to ~300 nM, $[Ca^{2+}]_i$ recovers with a kinetically simple time course,

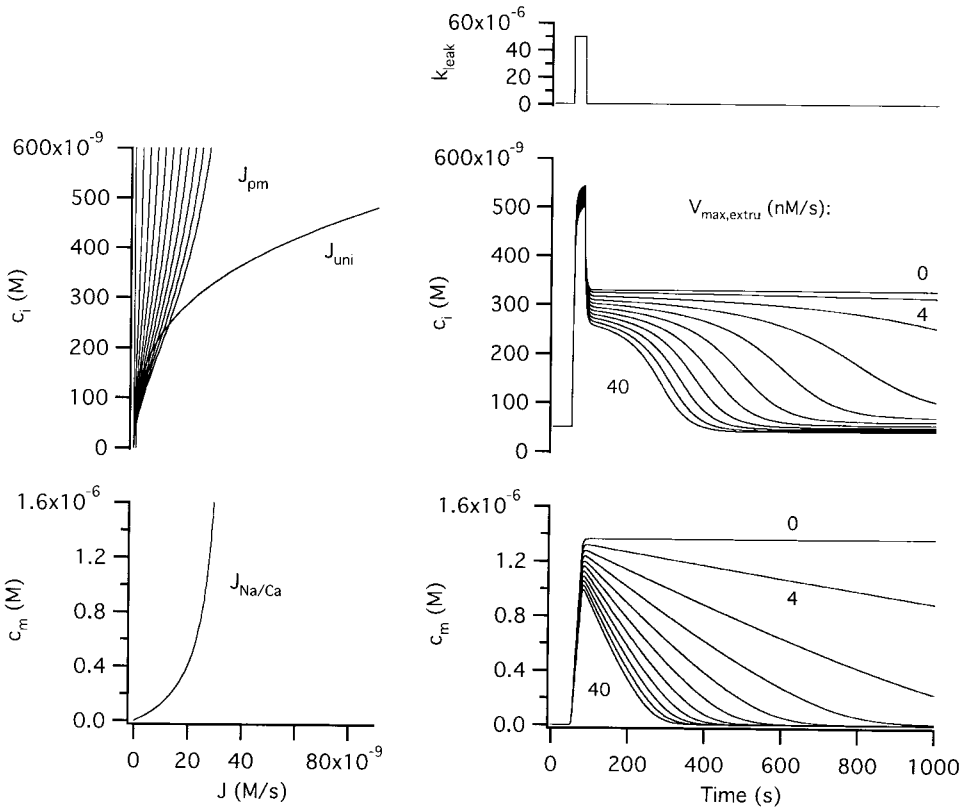

Figure 10. Role of Ca^{2+} extrusion during the plateau phase of the recovery. Family of responses elicited by a fixed stimulus with progressively lower rates of plasma membrane Ca^{2+} extrusion. As $V_{max,extru}$ is lowered, c_i and c_m both recover more slowly, indicating that the recovery is ultimately dependent on Ca^{2+} extrusion. As $V_{max,extru}$ approaches zero, the model cell approximates a closed system like classical preparations of isolated mitochondria in which Ca^{2+} transport only occurs between mitochondria and the extramitochondrial solution. In this limiting case, when the mitochondrial Ca^{2+} load is large enough to saturate the release pathway, extramitochondrial Ca^{2+} is maintained at a set point that depends on properties of the Ca^{2+} uptake and release pathways. For each simulation, $V_{max,extru}$ was initially set to 28.3 nM/s and was changed when the stimulus began. In the case $V_{max,extru} = 0$, k_{leak} was set to zero at the end of the stimulus to render the plasma membrane impermeable to Ca^{2+}.

while after longer trains that raise $[Ca^{2+}]_i$ to levels approaching ~500 nM, the recovery is kinetically complex, much like the recovery that follows a strong, steady depolarization (Friel and Tsien, 1994). Fig. 11 (left) compares simulated responses to repetitive stimulus trains of short and long duration. Since the interval between stimuli is too short to permit complete recovery, c_i undergoes temporal summation (see initial portion of the response to the longer stimulus train on an expanded time scale, right). As c_i rises, the rate of mitochondrial Ca^{2+} accumulation also rises (right, bottom). The properties of the recovery depend on the initial value of c_i and c_m, which in turn depend on stimulus duration. These simulations reproduce the differential effects of brief and long trains of evoked action potentials on $[Ca^{2+}]_i$ in these cells (Friel and Tsien, 1994).

DISCUSSION

Summary of Main Findings

Mitochondrial Ca^{2+} uptake and release pathways have been characterized in isolated mitochondria, but to our knowledge, the activity and $[Ca^{2+}]$ dependence of these transporters has not been described in intact cells. Such information is important because transport by isolated mitochondria may differ from that in situ, and because mitochondrial Ca^{2+} transport occurs within a system of transporters that must be taken into consideration.

This study extends to intact cells several general conclusions that have been drawn from studies of isolated mitochondria (Nicholls and Akerman, 1982; Hansford, 1985; Crompton, 1985, 1999). First, mitochondria are expected to accumulate Ca^{2+} even in response to weak stimuli that elevate $[Ca^{2+}]_i$ only slightly above resting levels. Second, there are two qualitatively different stimulus regimes. Weak stimuli raise $[Ca^{2+}]_i$ to a level where the rate of Ca^{2+} uptake is lower than the maximal rate of release via the Na^+/Ca^{2+} exchanger. Such stimuli would be expected to raise $[Ca^{2+}]_i$ and $[Ca^{2+}]_m$ to new steady state levels where the net Ca^{2+} flux across the plasma membrane and the net mitochondrial Ca^{2+} flux are both zero. Since the steady state value of $[Ca^{2+}]_i$ should not be influenced by mitochondrial Ca^{2+} transport, inhibitors of mitochondrial Ca^{2+} uptake (e.g., FCCP) should not affect this level; such inhibitors would, however, speed onset and recovery kinetics. This explains, at least in part, the paradoxical observation that although weak depolarizations increase total mitochondrial Ca concentration (Pivovarova et al., 1999) the steady $[Ca^{2+}]_i$ elevations they cause are not very sensitive to FCCP or CCCP (Friel and Tsien, 1994; Herrington et al., 1996). Strong stimuli, in contrast, raise $[Ca^{2+}]_i$ to levels where mitochondrial Ca^{2+} uptake exceeds the maximal rate of release so that a steady state is impossible. In this case, an apparent steady state can be reached where mitochondrial Ca^{2+} accumulation balances net Ca^{2+} entry across the plasma membrane. In this state, $[Ca^{2+}]_i$ is steadily ele-

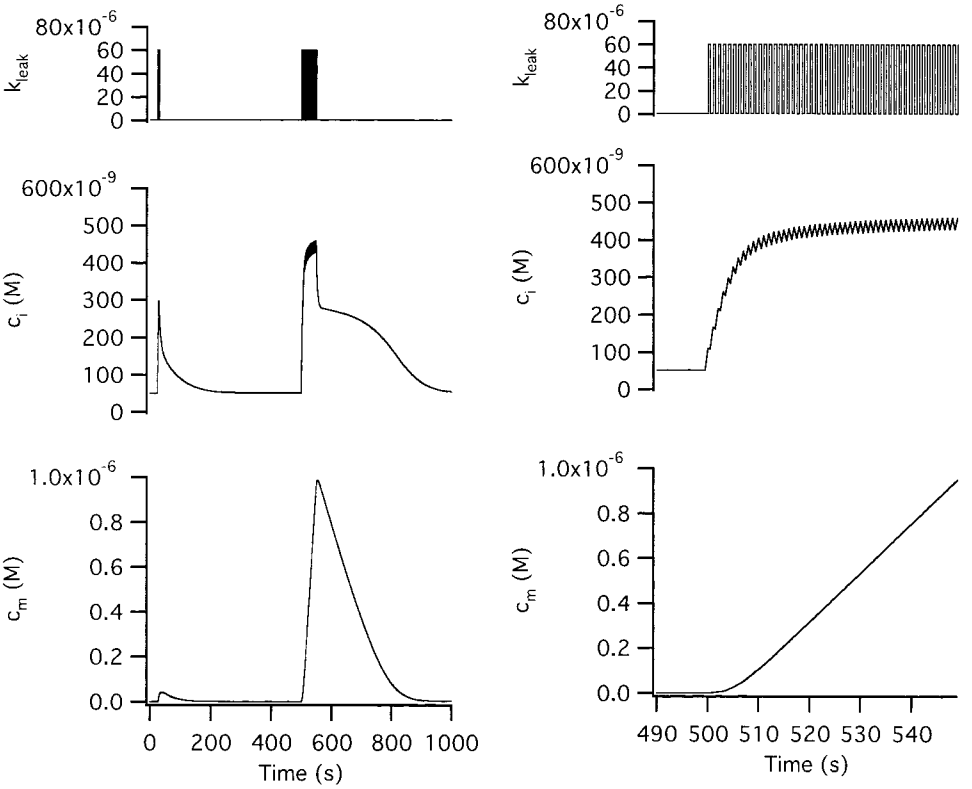

Figure 11. Responses to brief and long periodic stimulus trains. Comparison between the effects of brief and long periodic stimuli on c_i and c_m. When stimulus frequency is high enough so that recovery between individual stimuli is incomplete, temporal summation of c_i occurs. With a brief stimulus train, c_i does not rise high enough to produce appreciable mitochondrial Ca^{2+} accumulation so that the c_i recovery is largely unaffected by mitochondrial Ca^{2+} release. With a longer stimulus train that raises c_i to a level that causes significant mitochondrial Ca^{2+} accumulation, the rise in c_i is depressed and the recovery that follows the end of stimulation is marked by a prolonged multiphase recovery.

vated and mitochondria accumulate Ca^{2+} continuously, as seen during maintained depolarization (Pivovarova et al., 1999). Under these conditions of stimulation, inhibitors of mitochondrial Ca^{2+} uptake (e.g., FCCP) would shift the $[Ca^{2+}]_i$ level where J_{total} is zero to a higher level, accounting for the observation that strong depolarizations elicit larger $[Ca^{2+}]_i$ elevations after treatment with protonophores (Thayer and Miller, 1990). Interestingly, after blocking mitochondrial Ca^{2+} release, weak stimuli elicit responses like those produced by strong stimuli before block, characterized by continuous mitochondrial Ca^{2+} accumulation and a depressed steady $[Ca^{2+}]_i$ rise that is sensitive to Ca^{2+} uptake inhibitors.

Third, the $[Ca^{2+}]_i$ plateau level cannot be equated with the mitochondrial set point observed in studies of isolated mitochondria, since it depends jointly on mitochondrial and nonmitochondrial Ca^{2+} transport. Only in the limiting case where the plasma membrane is an impenetrable barrier to net Ca^{2+} transport can the plateau level be identified with the set point: in this case the model describes mitochondrial Ca^{2+} transport in a closed system like those used in studies of isolated mitochondria.

Finally, since $[Ca^{2+}]_i$ dynamics depends on a system of Ca^{2+} transport pathways, there are multiple sites for potential modulation of intracellular Ca^{2+} signals and the processes they control. For example, the simulations indicate that properties of the $[Ca^{2+}]_i$ recovery are jointly regulated by the mitochondrial Na^+/Ca^{2+} exchanger, Ca^{2+} uniporter and plasma membrane Ca^{2+} transport systems; they would also be influenced by ER Ca^{2+} transport if it were enabled (not shown).

Simplifications Used in the Analysis

Cells were studied under conditions that simplified the analysis of Ca^{2+} dynamics. Thapsigargin was used to inhibit Ca^{2+} transport by SERCA pumps, making it possible to study the interplay between Ca^{2+} transport across the plasma membrane and uptake and release by mitochondria in isolation from ER Ca^{2+} transport. Analysis was restricted to the recovery after depolarization-induced $[Ca^{2+}]_i$ elevations, after spatial $[Ca^{2+}]_i$ gradients are largely dissipated, so that the free Ca concentration within each cellular compartment is approximately uniform spatially. Extension of the analysis to include the ER will require quantitative information about its Ca^{2+} uptake and release pathways, while treating the initial period of stimulation, when Ca^{2+} is distributed nonuniformly, will require detailed information about the spatial distribution of mitochondria and its dynamics.

For the model simulations, Ca^{2+} entry was evoked by a step increase in plasma membrane Ca^{2+} permeability. This leads to an instantaneous increase in the rate of Ca^{2+} entry across the plasma membrane to a level that depends on both Ca^{2+} permeability and the difference between internal and external Ca^{2+} concentrations (see appendix). During stimulation, Ca^{2+} permeability was assumed to be constant, so time-dependent Ca^{2+} channel activation and inactivation were not taken into consideration. As a result, the simulated time courses of c_i and c_m during a depolarizing stimulus are not expected to follow precisely the changes in $[Ca^{2+}]_i$ and $[Ca^{2+}]_m$ that occur in situ. Information about the rate of Ca^{2+} entry during the stimulus should facilitate extension of the analysis to the period of depolarization.

Properties of Mitochondrial Ca^{2+} Uptake and Release in Intact Neurons

The equations describing mitochondrial Ca^{2+} uptake and release were motivated by results from studies of isolated mitochondria, so it is logical to compare, where possible, parameters of the equations with those describing transport by the isolated organelles. For J_{uni}, reliable estimates of $k_{max,uni}$ and $EC_{50,uni}$ were not possible given the limited $[Ca^{2+}]_i$ range over which our measurements were made. However, it was possible to estimate the Hill coefficient ($n_{uni} \sim 2$) which agrees with measurements from isolated mitochondria (Scarpa and Graziotti, 1973; Gunter and Pfeiffer, 1990). For $J_{Na/Ca}$ we obtained estimates of $V_{max,Na/Ca}$ that ranged from ~35–75 nM/s. This can be compared with the maximal rate of Na^+-dependent Ca^{2+} release by isolated heart and brain mitochondria (~10 and 30 nmol/mg prot/min; Hayat and Crompton, 1982; Gunter and Gunter, 1994), which convert to ~ 63–188 nmol/li cytosolic volume/s, values that are in reasonable agreement. The estimated value of $[Ca^{2+}]_m$ at which the rate of release is half maximal (~307 nM) is smaller than values obtained from studies of isolated mitochondria: ~1–10 μM (Gunter and Pfeiffer, 1990). With the estimated parameter values, the equations for J_{uni} and $J_{Na/Ca}$ together provide estimates of total mitochondrial Ca transport rates that agree with measured values. For example, with $k_{max,uni} = 80\ s^{-1}$ and $EC_{50,uni} = 10\ \mu M$, Eq. 2 can be evaluated at $[Ca^{2+}]_i = 554$ nM (the mean peak $[Ca^{2+}]_i$ level during steady 50 mM K^+ depolarization), to give $J_{uni} \sim 134$ nM/s. This converts to a total mitochondrial Ca flux of $(134)(200)/0.1 = 267\ \mu M/s$; after subtracting the (maximal) rate of Ca release (35 nM/s)$(200)/0.1 = 70\ \mu M/s$ gives a net flux (197 μM/s) that is similar to the measured rate of mitochondrial total Ca accumulation during exposure to 50 mM K^+, 184 μM/s (Pivovarova et al., 1999).

During all but the initial rapid phase of recovery, $J_{Na/Ca}$ depends on $\Delta[Ca^{2+}]_m^{(i)}$ in way that is consistent with previous studies (Wingrove and Gunter, 1986). However, during the initial phase, $J_{Na/Ca}$ increased in a way that could not be explained simply in terms of the accompanying rise in $\Delta[Ca^{2+}]_m^{(i)}$, suggesting that the rate of mitochondrial Ca^{2+} release depends on other factors

as well. Since previous work shows that $J_{Na/Ca}$ can be inhibited by high $[Ca^{2+}]_i$, the rate equation for $J_{Na/Ca}$ was modified to include an inhibitory term, after which it described $J_{Na/Ca}$ during the entire recovery. However, the steep $[Ca^{2+}]_i$ dependence of inhibition that was required seemed unrealistic (Hill coefficient ~6). This suggests that yet other variables may contribute to the depression of $J_{Na/Ca}$ under these conditions, for example, intramitochondrial Na concentration (Pivovarova et al., 1999). Therefore, the inhibitory factor should be regarded as an empirical description of the deviation of $J_{Na/Ca}$ from the simple rate equation. In any case, since simulated c_i and c_m dynamics were not modified appreciably by this factor, the depression of $J_{Na/Ca}$ during phase i of the recovery was not considered further.

Saturation of $J_{Na/Ca}$ strongly influences the way c_i and c_m change during and after stimulation. It sets the stage for continuous mitochondrial Ca^{2+} accumulation when c_i is high during stimulation, and it is responsible for a nearly constant rate of net Ca^{2+} release during phase ii of the recovery, which generates the c_i plateau. Ca^{2+} release could also occur at constant rate even when the release pathway is not saturated if Ca phosphate (CaP) formation effectively clamps intramitochondrial free Ca^{2+} concentration at a constant level (Nicholls and Akerman, 1982). This has been proposed to account for limited elevations in $[Ca^{2+}]_m$ during continuous electrical stimulation in nerve terminals (David, 1999). While such complexes form reversibly under the conditions of stimulation described in this study, and appear to play an important role in intramitochondrial Ca^{2+} buffering (Pivovarova et al., 1999), we did not see $J_{Na/Ca}$ fall abruptly from a ceiling during the recovery, arguing that such a mechanism is not responsible for the complex recovery kinetics described in this and the preceding study.

Mitochondrial Ca^{2+} Transport during Repetitive Electrical Activity

Based on the model simulations, the effect of repetitive stimulation on $[Ca^{2+}]_i$ and $[Ca^{2+}]_m$ would depend critically on stimulus frequency. If the interval between individual stimuli or bursts of stimuli is long enough to permit complete recovery, then $[Ca^{2+}]_i$ and $[Ca^{2+}]_m$ would change periodically. If the intervals are brief enough so that recovery is incomplete, both $[Ca^{2+}]_i$ and $[Ca^{2+}]_m$ would be expected to undergo temporal summation, ultimately oscillating about an elevated mean that increases with frequency. This could provide a mechanism by which fluctuations in $[Ca^{2+}]_i$ are translated into more steady elevations in $[Ca^{2+}]_m$. Indeed, this has been argued for the heart (Crompton, 1999). If a periodic stimulus causes average $[Ca^{2+}]_i$ to exceed the level where Ca^{2+} uptake by the uniporter is faster than the maximal rate of release, $[Ca^{2+}]_m$ will increase continuously, raising the possibility that there are distinct low and high frequency stimulus regimes analogous to the weak and strong regimes described above. Finally, slow net mitochondrial Ca^{2+} release in the aftermath of action potential-induced Ca^{2+} entry could provide a mechanism by which stimulus history influences responses to subsequent stimuli (Tang and Zucker, 1997).

APPENDIX

Equations Used to Describe the Components of the Total Ca^{2+} Flux

Ca^{2+} extrusion across the plasma membrane. J_{pm} was described by the sum of a linear leak flux (J_{leak}) and a saturable extrusion flux:

$$J_{pm} = J_{leak} + J_{extru} = k_{leak}([Ca^{2+}]_i - [Ca^{2+}]_o) + V_{max,extru} \Big/ \left\{1 + (EC_{50,extru}/[Ca^{2+}]_i)^{n_{extru}}\right\}, \quad (1)$$

where k_{leak} describes the Ca^{2+} permeability of the plasma membrane, $[Ca^{2+}]_o$ is the extracellular free Ca concentration, $V_{max,extru}$ is the maximal rate of Ca extrusion, $EC_{50,extru}$ is the $[Ca^{2+}]_i$ concentration where the Ca^{2+} extrusion rate is half maximal, and n_{extru} describes how steeply the extrusion rate increases with $[Ca^{2+}]_i$. Although the equation for the leak pathway does not explicitly include the voltage dependence of Ca^{2+} entry, it is consistent with the Goldman-Hodgkin-Katz flux equation if membrane potential is constant and the permeant ion is present at a much higher concentration in the extracellular solution than the intracellular solution. Note that according to this description, extrusion and leak fluxes are of opposite sign as long as $[Ca^{2+}]_i < [Ca^{2+}]_o$ and that J_{pm} is zero when the magnitudes of the component fluxes are equal.

Mitochondrial Ca^{2+} uptake. J_{uni} Mitochondrial Ca^{2+} uptake was described by:

$$J_{uni} = k_{uni,max}[Ca^{2+}]_i \Big/ \left\{1 + (EC_{50,uni}/[Ca^{2+}]_i)^{n_{uni}}\right\}, \quad (2)$$

where $k_{uni,max}$ is the limiting slope at high $[Ca^{2+}]_i$, $EC_{50,uni}$ is the value of $[Ca^{2+}]_i$ where activation of uptake is half-maximal and n_{uni} is a Hill coefficient. Eq. 2 would describe the total Ca^{2+} flux carried by a population of channels whose open probability increases with $[Ca^{2+}]_i$ and which, when open, permit Ca^{2+} to flow unidirectionally at a rate that depends on $[Ca^{2+}]_i$ and the magnitude of a constant electric field. This conforms with expectations from the Goldman-Hodgkin-Katz flux equation under conditions where mitochondrial membrane potential is constant, intramitochondrial Ca^{2+} concentration is low compared with $[Ca^{2+}]_i$, and

the permeation pathway is far from saturation. In this case, $k_{uni,max}$ would depend on mitochondrial membrane potential. Since there was no indication that J_{uni} was limited over the range $[Ca^{2+}]_i < 1$ μM, parameters for Eq. 2 were estimated as follows. n_{uni} was determined as the slope of a line fitted to a plot of $\log(k_{uni,max}[Ca^{2+}]_i/J_{uni} - 1)$ vs $\log([Ca^{2+}]_i)$. This provided estimates of n_{uni} that were quite insensitive to $k_{uni,max}$ over the range (10 − 1000 s^{-1}). After determining n_{uni}, $k_{uni,max}$ was determined by fitting Eq. 2 to J_{uni} data while holding n_{uni} constant and setting $EC_{50,uni}$ to 10 μM (Gunter and Pfeiffer, 1990).

Mitochondrial Ca^{2+} release: $J_{Na/Ca}$. The rate of Ca release via the Na^+/Ca^{2+} exchanger was described by a saturable function of $[Ca^{2+}]_m$:

$$J_{Na/Ca} = -V_{max,Na/Ca}/(1 + EC_{50,Na/Ca}/[Ca^{2+}]_m), \quad (3)$$

where $V_{max,Na/Ca}$ is the maximal rate of Ca^{2+} release and $EC_{50,Na/Ca}$ is the value of $[Ca^{2+}]_m$ at which release rate is half maximal. The Na^+ concentration is not explicitly taken into consideration since changes in $[Na^+]_i$ and $[Na^+]_m$ induced by depolarizations up to ~20 s are small (Pivovarova et al., 1999). Therefore, $V_{max,Na/Ca}$ is regarded as a constant that depends on both $[Na^+]_i$ and $[Na^+]_m$ and possibly membrane potential (Jung et al., 1995). Eq. 3 was expressed in terms of the measured integrated net mitochondrial Ca^{2+} flux $\Delta[Ca^{2+}]_m^{(i)}$:

$$\Delta[Ca^{2+}]_m^{(i)}(t) = \int_{\infty}^{t} J_{mito}\,dt'$$
$$= \gamma\{[Ca^{2+}]_m(t) - [Ca^{2+}]_m(\infty)\}$$
$$= \gamma\Delta[Ca^{2+}](t)_m. \quad (4)$$

This was done by writing $[Ca^{2+}]_m$ in terms of $\Delta[Ca^{2+}]_m^{(i)}$ as follows (Eq. 5):

$$[Ca^{2+}]_m(t) = \Delta[Ca^{2+}]_m^{(i)}(t)/\gamma + [Ca^{2+}]_m(\infty), \quad (5)$$

where $[Ca^{2+}]_m(\infty)$ is the resting value of $[Ca^{2+}]_m$ and γ is the ratio of effective mitochondrial and cytosolic volumes. Substituting into Eq. 3 gives (Eq. 6):

$$J_{Na/Ca} = -V_{max,Na/Ca}/$$
$$\{1 + EC_{50,Na/Ca}/(\Delta[Ca^{2+}]_m^{(i)}/\gamma + [Ca^{2+}]_m(\infty))\}. \quad (6)$$

This equation can be written as a function of $\Delta[Ca^{2+}]_m^{(i)}$ and three parameters:

$$J_{Na/Ca} = -A/\{1 + 1/(\Delta[Ca^{2+}]_m^{(i)}/B + C)\}. \quad (7)$$

where $A = V_{max,Na/Ca}$, $B = \gamma EC_{50,Na/Ca}$, and $C = [Ca^{2+}]_m(\infty)/EC_{50,Na/Ca}$. Eq. 7 was fit to data shown in Fig. 2 F during the plateau phase of the recovery to obtain estimates of $V_{max,Na/Ca}$ and the lumped parameters $\gamma EC_{50,Na/Ca}$ and $[Ca^{2+}]_m(\infty)/EC_{50,Na/Ca}$. The steep decline in $J_{Na/Ca}$ at high $\Delta[Ca^{2+}]_m^{(i)}$ can be described by multiplying by an inhibitory factor to give $J_{Na/Ca}'$:

$$J_{Na/Ca}' = \delta([Ca^{2+}]_i)J_{Na/Ca}, \quad (8)$$

where (Eq. 9)

$$\delta([Ca^{2+}]_i) = 1 - 1/\left\{1 + (K_{d,inhib}/[Ca^{2+}]_i)^{n_{inhib}}\right\}, \quad (9)$$

where $K_{d,inhib}$ is the concentration for half maximal inhibition by cytosolic Ca^{2+} and n_{inhib} describes the steepness of inhibition by $[Ca^{2+}]_i$.

Description of the Model

The experimentally determined rate laws for J_{pm}, J_{uni}, and $J_{Na/Ca}$ provided all the flux definitions for a one-pool model of Ca^{2+} dynamics (Friel and Tsien, 1994). Dynamics of the free Ca^{2+} concentration within the cytosol (c_i) and the mitochondrial pool (c_m) were described by the following differential equations (Eqs. 10 and 11):

$$dc_i/dt = -(J_{pm} + J_{mito}) \quad (10)$$

$$dc_m/dt = J_{mito}/\gamma, \quad (11)$$

where the concentration fluxes (nM/s, referred to cytosolic effective volume) are (Eqs. 12–18):

$$J_{pm} = J_{leak} + J_{extru}, \quad (12)$$

$$J_{mito} = J_{uni} + J_{Na/Ca}, \quad (13)$$

$$J_{leak} = k_{leak}(c_i - c_o), \quad (14)$$

$$J_{extru} = V_{max,extru}/[1 + (EC_{50,extru}/c_i)^{n_{extru}}], \quad (15)$$

$$J_{uni} = k_{max,uni}c_i/[1 + (EC_{50,uni}/c_i)^{n_{uni}}], \quad (16)$$

$$J_{Na/Ca} = -V_{max,Na/Ca}/[1 + (EC_{50,Na/Ca}/c_m)], \quad (17)$$

$$\gamma = (v_m\kappa_m^T/v_i\kappa_i^T), \quad (18)$$

where k_{leak}, $V_{max,extru}$, $EC_{50,extru}$, n_{extru}, $k_{max,uni}$, $EC_{50,uni}$, n_{uni}, $V_{max,Na/Ca}$, and $EC_{50,Na/Ca}$ are constants described above, and c_o is the (constant) extracellular Ca^{2+} concentration. Note that Eqs. 12–17 describe concentration fluxes that can be interpreted as the rate of Ca^{2+} delivery by the individual transport systems (e.g., $\tilde{J}_{pm}$) divided by the effective cytoplasmic volume (e.g., $J_{pm} = \tilde{J}_{pm}/(v_i\kappa_i^T)$) where v_i is the cytoplasmic volume

and κ_i^T is the ratio of (infinitesimal) changes in total to free Ca concentration. This model does not explicitly include a description of mitochondrial membrane potential ($\Delta\psi$) dynamics and applies to the case where $\Delta\psi$ is constant (see Magnus and Keizer, 1997 for a description of the more general case).

To simulate the effects of membrane depolarization, k_{leak} was increased by Δk_{leak}. According to Eq. 14, this would instantaneously increase the rate of Ca^{2+} entry by $\Delta k_{leak}(c_i - c_o)$. For example, this could describe rapid activation of non-inactivating Ca^{2+} channels in the case where permeation occurs at steady membrane potential and conforms with constant field theory with $c_i << c_o$ (Friel, 1995). In this case, Δk_{leak} would depend on membrane potential. To include inhibitory effects of cytosolic Ca^{2+} on $J_{Na/Ca}$, Eq. 17 was modified as follows:

$$J_{Na/Ca}' = -\delta(c_i)V_{max,\,Na/Ca}/[1 + (EC_{50,\,Na/Ca}/c_i)], \quad (19)$$

where $\delta(c_i)$ is given by Eq. 20:

$$\delta(c_i) = 1 - 1/[1 + (K_{inhib}/c_i)^{n_{inhib}}]. \quad (20)$$

This work was supported by grants from the American Heart Association (96011490) and from the National Institutes of Health (NS 33514-03).

Submitted: 23 September 1999
Revised: 30 December 1999
Accepted: 5 January 2000
Released online: 28 February 2000

REFERENCES

Babcock, D.F., J. Herrington, P.C. Goodwin, Y.B. Park, and B. Hille. 1997. Mitochondrial participation in the intracellular Ca^{2+} network. *J. Cell Biol.* 136:833–844.

Boyce, W.E., and R.C. DiPrima. 1969. Elementary differential equations. John Wiley & Sons, Inc., New York, NY. 353–357.

Crompton, M. 1985. The regulation of mitochondrial calcium transport in heart. *Curr. Top. Memb. Trans.* 25:231–276.

Crompton, M. 1999. The mitochondrial permeability transition pore and its role in cell death. *Biochem. J.* 341:233–249.

David, G. 1999. Mitochondrial clearance of cytosolic Ca^{2+} in stimulated lizard motor nerve terminals proceeds without progressive elevation of mitochondrial matrix $[Ca^{2+}]$. *J. Neurosci.* 19:7495–7506.

Friel, D.D. 1995. $[Ca^{2+}]_i$ oscillations in sympathetic neurons: an experimental test of a theoretical model. *J. Biophys.* 68:1752–1766.

Friel, D.D., and R.W. Tsien. 1994. An FCCP-sensitive Ca^{2+} store in bullfrog sympathetic neurons and its participation in stimulus-evoked changes in $[Ca^{2+}]_i$. *J. Neurosci.* 14:4007–4024.

Gunter, K.K., and T.E. Gunter. 1994. Transport of calcium by mitochondria. *J. Bioenerg. Biomem.* 26:471–485.

Gunter, T.E., and D.R. Pfeiffer. 1990. Mechanisms by which mitochondria transport calcium. *Am. J. Physiol.* 258:C755–C786.

Hansford, R.G. 1985. Relation between mitochondrial calcium transport and control of energy metabolism. *Rev. Physiol. Pharmacol.* 102:1–72.

Hayat, L.H., and M. Crompton. 1982. Evidence for the existence of regulatory sites for Ca^{2+} on the Na^+/Ca^{2+} carrier of cardiac mitochondria. *Biochem. J.* 202:509–518.

Herrington, J., Y.B. Park, D.F. Babcock, and B. Hille. 1996. Dominant role of mitochondria in clearance of large Ca^{2+} loads from rat adrenal chromaffin cells. *Neuron.* 16:219–228.

Hernandez-Cruz, A., F. Sala, and P.R. Adams. 1990. Subcellular calcium transients visualized by confocal microscopy in a voltage-clamped vertebrate neuron. *Science.* 247:858–862.

Horikawa, Y., A. Goel, A.P. Somlyo, and A.V. Somlyo. 1998. Mitochondrial calcium in relaxed and tetanized myocardium. *Biophys. J.* 74:1579–1590.

Hua, S.Y., M. Nohmi, and K. Kuba. 1993. Characteristics of Ca^{2+} release induced by Ca^{2+} influx in cultured bullfrog sympathetic neurons. *J. Physiol.* 464:245–272

Jung, D.W., K. Baysal, and G.P. Brierly. 1995. The sodium-calcium antiport of heart mitochondria in not electroneutral. *J. Biol. Chem.* 270:672–678.

Magnus, G., and J. Keizer. 1997. Minimal model of β-cell mitochondrial Ca^{2+} handling. *Am. J. Physiol.* 273:C717–C733.

Moravec, C.S., and M. Bond. 1992. Effect of inotropic stimulation on mitochondrial calcium in cardiac muscle. *J. Biol. Chem.* 267: 5310–5316.

Nicholls, D.G. 1985. A role for the mitochondrion in the protection of cells against calcium overload. *Prog. Brain Res.* 63:97–106.

Nicholls, D., and K. Akerman. 1982. Mitochondrial calcium transport. *Biochim. Biophys. Acta.* 683:57–88

Pivovarova, N.B., J. Hongpaisan, S.B. Andrews, and D.D. Friel. 1999. Depolarization-induced mitochondrial Ca accumulation in sympathetic neurons: spatial and temporal characteristics. *J. Neurosci.* 19:6372–6384.

Rizzuto, R., P. Pinton, W. Carrington, F.S. Fay, K.E. Fogarty, L.M. Lifshitz, R.A. Tuft, and T. Pozzan. 1998. Close contacts with the endoplasmic reticulum as determinants of mitochondrial Ca^{2+} responses. *Science.* 280:1763–1766.

Scarpa, A., and P. Graziotti. 1973. Mechanisms for intracellular calcium regulation in heart. *J. Gen. Physiol.* 62:756–772.

Tang, Y., and R.S. Zucker. 1997. Mitochondrial involvement in post-tetantic potentiation of synaptic transmission. *Neuron.* 18:483–491.

Thayer, S.A., and R.J. Miller. 1990. Regulation of the intracellular free calcium concentration in single rat dorsal root ganglion neurones in vitro. *J. Physiol.* 425:85–115.

Wingrove, D.E., and T.E. Gunter. 1986. Kinetics of mitochondrial calcium transport. *J. Biol. Chem.* 261:15166–15171.